LA-7310

Tritium Production in a Sphere of ^{6}LiD Irradiated by 14-MeV Neutrons

LOS ALAMOS SCIENTIFIC LABORATORY

Post Office Box 1663 Los Alamos. New Mexico 87545

An Affirmative Action/Equal Opportunity Employer

UNITED STATES
DEPARTMENT OF ENERGY
CONTRACT W-7405-ENG. 36

LA-7310
UC-34c
Issued: October 1978

Tritium Production in a Sphere of ^{6}LiD Irradiated by 14-MeV Neutrons

A. Hemmendinger
C. E. Ragan
E. R. Shunk
A. N. Ellis
J. M. Anaya
Jon M. Wallace

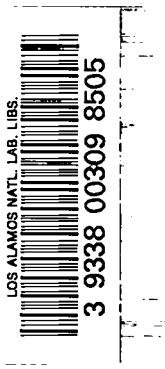

CONTENTS

PART II
CALCULATIONS OF TRITIUM PRODUCTION AND RADIOCHEMICAL ACTIVATION IN A SPHERE OF ^{6}LiD IRRADIATED BY 14-MeV NEUTRONS

TRITIUM PRODUCTION IN A SPHERE OF ^{6}LiD IRRADIATED BY 14-MeV NEUTRONS

by

A. Hemmendinger, C. E. Ragan, E. R. Shunk,
A. N. Ellis, J. M. Anaya, and Jon M. Wallace

ABSTRACT

The specific production of tritium in samples of ^{6}LiH and ^{7}LiH embedded in a 600-mm-diam sphere of ^{6}LiD irradiated by a central source of 14-MeV neutrons has been determined by measuring the activity of the hydrogen evolved from the samples of each isotope at each of five different radii in the ^{6}LiD assembly. The entire process of decomposing the LiH, transferring the evolved gas into counters, and determining the decay rate was standardized by processing LiH samples irradiated by thermal neutrons for which the ^{6}Li(n,α) cross section is well known.

The specific production of tritium in ^{6}LiH and ^{7}LiH (embedded samples) and the activation of radiochemical detector foils of ^{45}Sc, ^{89}Y, ^{90}Zr, ^{169}Tm, ^{191}Ir$_{.373}$ ^{193}Ir$_{.627}$, ^{197}Au, ^{238}U, and ^{236}U placed at various positions in the ^{6}LiD sphere have been calculated and compared with the experimental data. One- and three-dimensional Monte Carlo and S_n neutron-transport calculations were performed. The most reliable (three-dimensional Monte Carlo) calculation is in reasonable agreement with both the tritium-production and the radiochemical-activation data. The existing discrepancies between calculation and experiment appear largely attributable to uncertainties in some tritium-production and radiochemical-activation cross sections.

PART I

MEASUREMENT OF TRITIUM PRODUCTION IN A SPHERE OF ^{6}LiD IRRADIATED BY 14-MeV NEUTRONS

by

A. Hemmendinger, C. E. Ragan, E. R. Shunk,
A. N. Ellis, and J. M. Anaya

ABSTRACT

The specific production of tritium in a 600-mm-diam sphere of ^{6}LiD irradiated by a central source of 14-MeV neutrons has been determined by measuring the activity of the tritium in samples of ^{6}LiH and ^{7}LiH contained in sealed quartz ampules embedded in the sphere. Results are reported for several samples of each isotope at each of five different radii in the assembly. The entire process of decomposing the LiH samples, transferring the evolved gas into counters, and determining the decay rate was standardized by processing LiH samples irradiated by thermal neutrons for which the ^{6}Li(n,α) cross section is well known.

I. INTRODUCTION

The determination of the amount of tritium produced in a blanket of lithium surrounding a neutron source has long been of interest in connection with nuclear weapons and controlled thermonuclear reactors. If a sustained thermonuclear reaction requires tritium as a fuel, the only plausible way to keep such a system operating would be to create tritium as a by-product of 14-MeV neutrons produced in the reactor. In 1958 Marvin Wyman[1] reported the tritium production in samples of ^{7}Li metal embedded in a 600-mm-diam sphere of LiD surrounding a source of 14-MeV neutrons. His results confirmed that tritium is indeed produced in substantial quantities by the reaction ^{7}Li(n,n'α).

Several measurements of tritium production in blankets containing natural lithium are shown to be in fair agreement with calculations.[2-4] Muir and Wyman[5] and Qaim, Wölfle, and Stöcklin[6] have discussed the need for integral data on tritium production, and they have analyzed earlier experiments.

We report here an experiment, similar to Wyman's, in which we irradiated an assembly of ^{6}LiD containing test samples of ^{6}LiH and ^{7}LiH. Teledyne Isotopes, Inc., Westwood, NJ 07675, analyzed these samples by evolving hydrogen from them and counting the tritium decay by a method resembling, but developed independently of, that described by Qaim.[7] Our experiment, which was designed to investigate the transport of neutrons in ^{6}LiD and to determine the tritium production, provides benchmark measurements for comparison with calculations. Results for tritium production in ^{7}Li in such an assembly have not previously been reported.

II. THE ^{6}LiD ASSEMBLY

Nesting hemispherical shells of ^{6}LiD were constructed to fit around the target assembly of a Cockcroft-Walton (C-W) accelerator. The inside and outside diameters of the assembly were 44.4 and 600

mm. Details of dimensions, masses, and isotopic composition are given in Table I. Small cavities at the shell interfaces held samples of ^{6}LiH and ^{7}LiH; these samples were in sealed quartz ampules (Fig. 1) in two sizes: 10-mm o.d. for the two inner-shell interfaces and 18-mm o.d. for the outer shells. The ampules were filled, weighed, and sealed in an atmosphere of helium.* All ampules were taped in place in the assembly, as shown in Fig. 2. At least two empty ampules (treated in the same manner as the filled ampules) were positioned at each radius for background measurements.

The neutron-source flux distribution was measured over 4π sr using both liquid-scintillator

*All ^{6}LiD parts and LiH samples were prepared by Union Carbide Corporation, Oak Ridge, TN 37830.

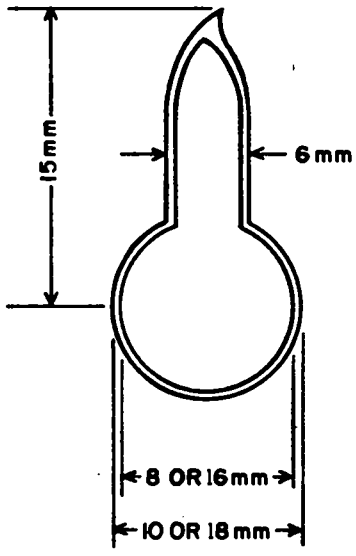

Fig. 1.
Quartz ampule, with dimensions for two sizes, which held the lithium hydride samples for irradiation.

TABLE I

SPECIFICATIONS FOR ^{6}LID HEMISPHERICAL SHELLS

Diameter (mm)		Mass	^{6}Li	
Inside	Outside	(kg)	(at.%)	(wt%)
44.4	100.0	0.1783	95.59	94.89
		0.151		
102.0	152.3	0.449	95.59	94.89
		0.490		
154.3	252.0	2.465	95.59	94.89
		2.330		
254.0	400.0	9.133	95.68	95.00
		9.430		
402.0	600.0	30.000	95.68	95.00
		29.200		
Total mass =		83.826		

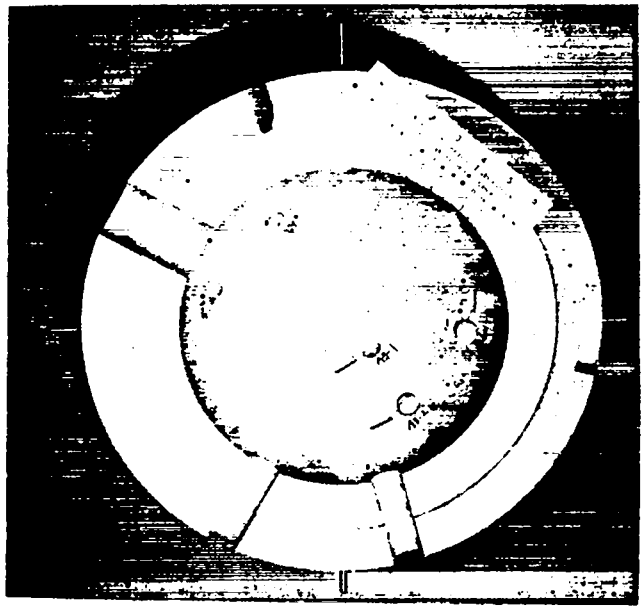

Fig. 2.
Lithium hydride samples taped in place in cavities in the ^{6}LiD hemishell.

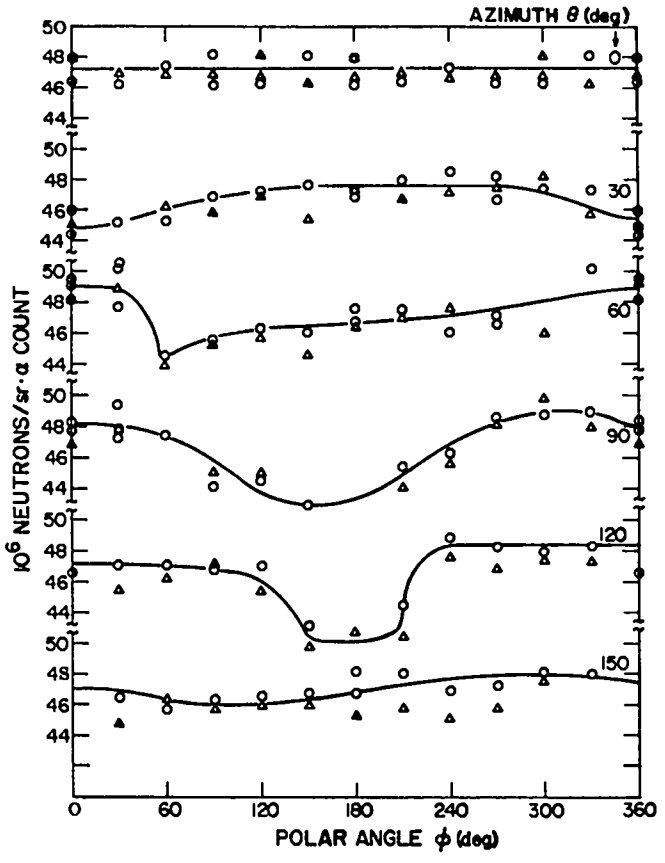

Fig. 3.
Map of the neutron flux over the sphere around the C-W machine target. The measurements made using a NE-213 (Nuclear Enterprises, Inc.) scintillator biased at 12 MeV are shown as circles, and those obtained using a cadmium-shielded ^{238}U fission detector are shown as triangles.

and fission detectors. This distribution is displayed in Fig. 3 as a function of the azimuthal angle θ (0° being the direction of the deuteron beam) and the polar angle ϕ, the angular displacement about the axis defined by the deuteron beam (0° being in the horizontal plane to the right side looking into the beam). The observed flux distribution is not quite isotropic because of a superposition of two effects: (a) neutron emission from the recoiling compound nucleus varies relative to the 90° flux by +5% in the forward direction to −5% in the backward direction and (b) the flux is attenuated by about 10% in directions in which neutrons traverse the target backing.

The copper target wafer, which had a surface layer of tritium embedded in titanium, was oriented in a vertical plane at an angle 45° from the direction of the horizontal deuteron beam. The ^{6}LiH samples in the assembly were located in the vertical −110° plane (B-B), the ^{7}LiH in the vertical −65° plane (A-A), as shown in Fig. 4. The location of a sample in either plane is specified by its radius r and by a polar angle ω measured from the parting plane looking into the beam. Care was taken in positioning the samples to avoid locations at which there might be a neutron flux perturbation; thus no two ampules were placed along the same radius, near the parting plane of the sphere, or in the plane of the C-W target where there are flux perturbations as large as ±8%. These precautions were taken even though variations in the flux were probably smoothed out at distances greater than one mean free path in the ^{6}LiD—108 mm for 14-MeV neutrons.

Figure 5 shows the lower half of the assembly in place around the target, and Fig. 6 shows the partially completed ^{6}LiD assembly. The assembly was supported in a 520-mm-diam hole in a 6.4-mm-thick circular aluminum plate. The plate was suspended from an assembly frame (Fig. 7) constructed to mount massive objects around the C-W machine target.

III. STANDARDIZATION

A. General Procedure

To evolve hydrogen from lithium hydride, Teledyne crushed each quartz ampule in a stainless steel tube that they heated until there was no further evolution of gas. The volume of the evolved hydrogen was measured, and hydrogen carrier was added to the small samples only. The hydrogen gas was converted to water, and the water was diluted and divided into several parts in measured ratios. To assay one of these subdivided samples, they converted it back to hydrogen and transferred the gas into a shielded proportional counter.

In addition, a portion of the tritiated water from each sample was mixed with a liquid scintillator, and the sample count rate was determined. Teledyne calibrated the counting system routinely by counting part of a standard sample, NBS 4925,

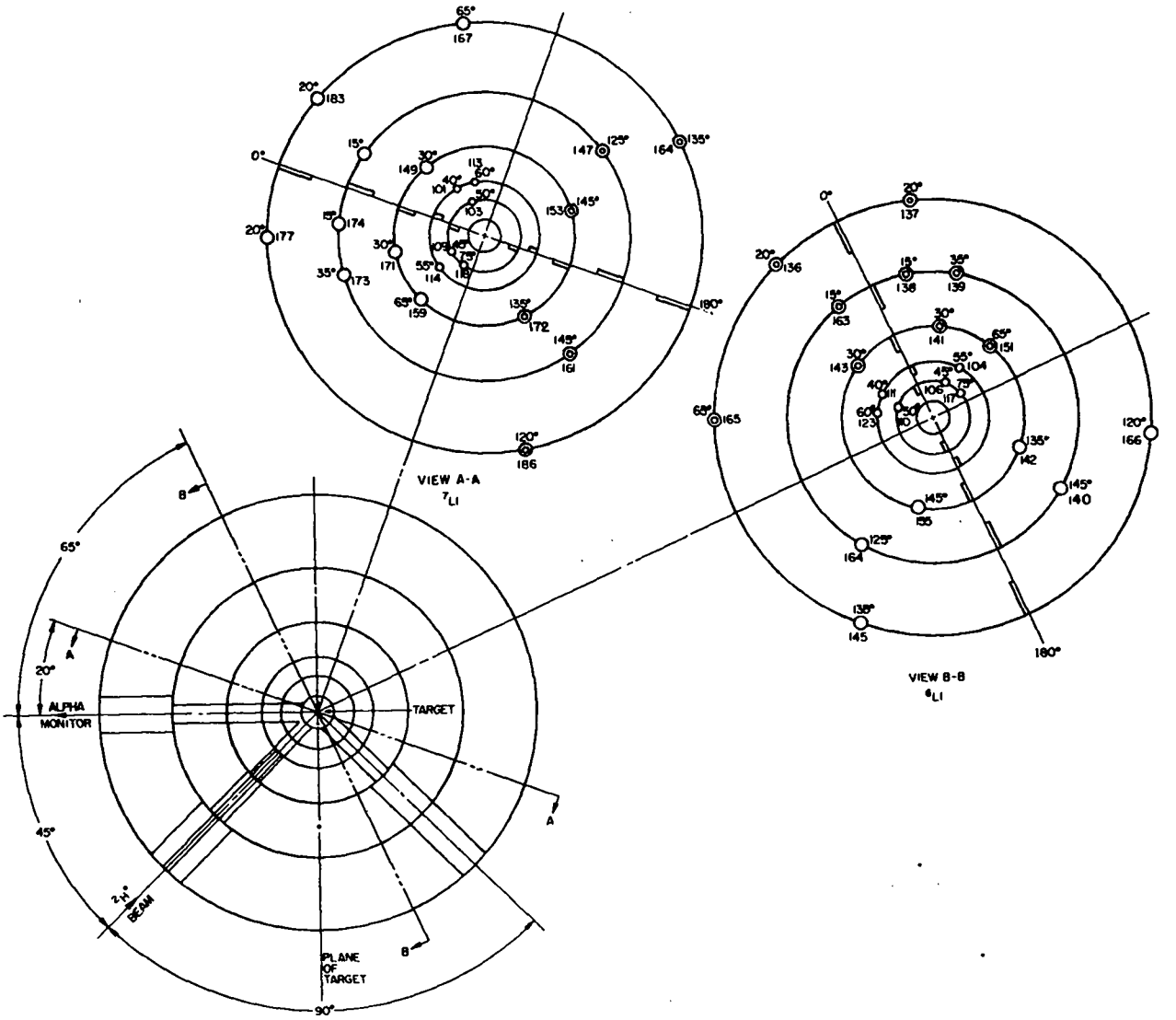

Fig. 4.

Schematic showing positions of lithium hydride samples in the ^{6}LiD assembly. The small circles for some samples indicated that the stem of the ampule is toward the observer. The angles above the parting plane are negative.

which they had used for about 10 years; this provided Teledyne's primary standard. They used two additional calibration methods:

(1) counting a fraction of NBS 4926 standard sample, which had been calibrated by the National Bureau of Standards on 1 July 1976;

(2) comparing Teledyne's count on a fraction of our sample 327 with NBS's count on another fraction of the same sample.

A comparison of calibrations 1 and 2 (Table II) shows that the Teledyne and NBS determinations of tritium activity agree within 1.5%, which is within Teledyne's standard deviation. NBS estimates their systematic error at 2%; this is the same systematic error inherent in the Teledyne measurements, because both groups used fractions of the same tritium standard source.

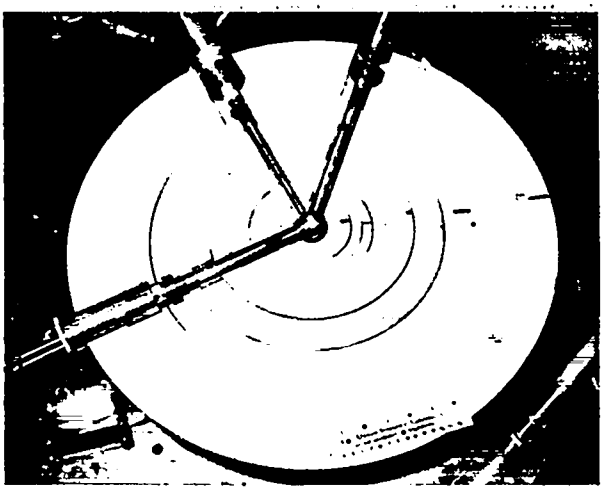

Fig. 5.
Bottom half shells of the ^6LiD assembly mounted around the target of the C-W machine. The tube at the lower left is for target insertion and cooling; at upper left is the beam entry tube, and at upper right is the alpha-particle counter tube for monitoring the neutron flux.

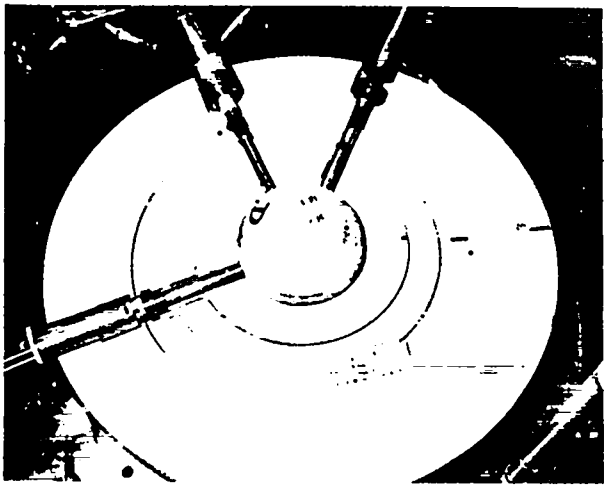

Fig. 6.
Shells of ^6LiD mounted around the tritium target of the C-W machine. The bottom half of the assembly is complete; the outer top three hemishells are missing.

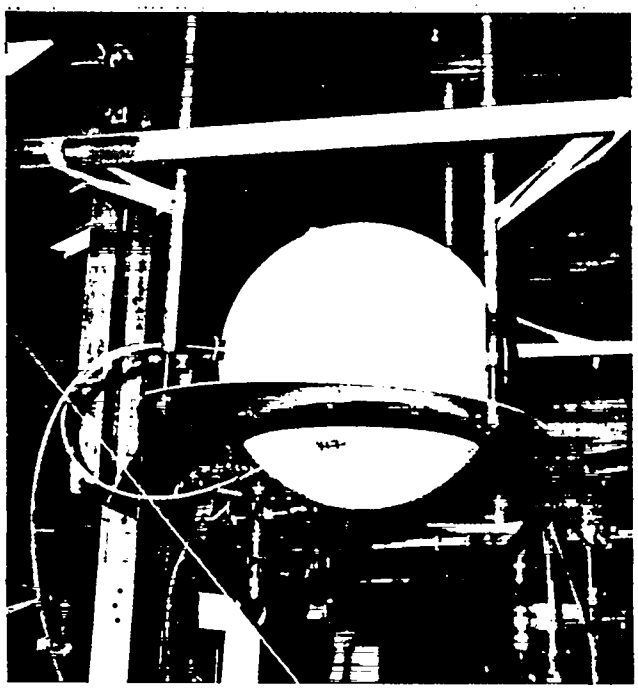

Fig. 7.
Completed ^6LiD assembly surrounding the target of the C-W machine. The aluminum circular mounting plate is suspended from a pneumatic assembly machine by three rods. Three sample ampules can be seen on the outside surface.

Because there may be other systematic errors, which we believe are associated with gas handling by Teledyne (see Sec. III.E), tritium production results in lithium hydride irradiated by thermal neutrons were used to calibrate the whole process of gas handling and counting. These lithium hydride samples, each containing a gold fluence monitor, were irradiated in the thermal column of the Los Alamos Scientific Laboratory (LASL) Omega West Reactor. The ratio of the thermal capture cross section of ^6Li to that of ^{197}Au is well enough known[5,6] that tritium counting by Teledyne of these reactor-irradiated samples provided a calibration of Teledyne's measurements relative to the absolute counting of the gold by LASL.

TABLE II

COMPARISON OF TRITIUM DETERMINATIONS IN WATER BY TELEDYNE AND NBS

Sample	Ref. Date	Teledyne Measurement [10^3 dis·s^{-1}·(g H_2O)$^{-1}$]	NBS Measurement [10^3 dis·s^{-1}·(g H_2O)$^{-1}$]	Ratio T/NBS
NBS H-3	8/16/76	2.242		
		2.292		
		av = 2.267	2.276	0.9960
LASL-327	10/11/76	1.960	1.944	1.0083

B. Backgrounds

A surprise came in our investigation of samples of LiD, the material that we originally intended to use in the ampules, for they had tritium backgrounds high compared with the activation expected in the C-W irradiations. For completeness, we report these background levels in Appendix A. Inasmuch as the deuterium abundance in our LiD was typically 99.9 at.%, it is reasonable to suppose that an increase of the deuterium content by a factor of 7000 above the natural level will necessarily increase the tritium fraction of hydrogen even more; the natural abundance of tritium augmented by enrichment appears sufficient to account for the observed backgrounds. In our samples of ^{6}LiH, the tritium background was below Teledyne's detection limit; the samples of ^{7}LiH contained appreciably more tritium, but never more than a few per cent of the activity induced by irradiation. Measured ^{7}LiH backgrounds are listed in Table III.

TABLE III

TRITIUM ACTIVITY IN UNIRRADIATED AMPULES OF ^{7}LiH

Sample No.	Mass ^{7}LiH (g)	Tritium Decay Rate [dis·s^{-1}·(g LiH)$^{-1}$]
125	0.1467	2.317
127	0.1589	4.900
128	0.1694	3.250
179	1.0125	2.750
176	1.0059	2.667
182	0.9501	3.250
189	1.0028	3.600
190	1.0027	3.516
316	0.8982	3.583
322	1.0683	8.617
323	1.0871	3.100
		av = 3.78 ± 0.52

C. Thermal Activations of LiH

The test samples of lithium hydride irradiated in the thermal flux contained a low concentration of ^{6}Li (about 0.1%) to limit perturbation of the neutron flux by absorption in the sample. Even so, the ^{6}Li and ^{1}H in the samples produced a combined flux depression, with approximately equal contributions, of about 5%, a depression for which we could adequately correct.

The gold fluence monitor obviously should have been uniformly distributed in the sample, but we found no way to do this. Gold powder settled quickly to the bottom of the ampule, and the use of solutions promised to add more problems than it solved. In each ampule we placed a sample of approximately 10 mg of 0.05-mm-diam gold wire wound in a helix on a 1.6-mm-diam mandrel. The helix was stretched axially to span the inside diameter of the ampule (about 8 or 16 mm for the two sizes of ampules), and we attempted to locate the helix along the axis of the fill tube. X-radiographs of the filled ampules showed that not all helixes were collinear with the fill tube, but we judged consequent errors in fluence measurement to be negligible.

D. Gamma-Ray Counting of ^{196}Au

We counted the 412-keV gamma rays from the activated gold in the samples with a Ge(Li) detector. To eliminate small errors in ampule shapes and placements, each sample was rotated at 0.1 rev/s while it was counted. The sample holder was mounted rigidly and reproducibly by a clamp around the case of the Ge(Li) detector, as shown in Fig. 8. We calibrated the gamma-ray detector by placing standard sources in the same sample mounting. One standard source* was ^{152}Eu, which has, by coincidence, a 412-keV line. A second standard source was a few milligrams of activated gold wire that LASL radiochemists (Group CNC-11) counted in a NaI(Tl) well detector and also with a Ge(Li) detector. Both of these counters were calibrated with a NBS mixed radionuclide emission rate standard.

*Purchased from Laboratoire de Métrologie des Rayonnements Ionisants, Commissariat a l'Energie Atomique, Saclay, France.

Fig. 8.
Rotating sample holder mounted on the Ge(Li) detector that was used to detect the 412-keV gamma rays from test samples activated by thermal neutrons.

E. Calculation of Expected Tritium Activity

To determine the relation between the predicted tritium decay rate dN_1/dt and the number of ^{196}Au gamma rays counted, we note that the net production rate of tritium is

$$\frac{dN_1}{dt} = N_{Li\text{-}6}\sigma_1\phi - \lambda_1 N_1 \quad , \tag{1}$$

where σ_1 is the thermal cross section for ^{6}Li(n,α), λ_1 is the decay constant for tritium, and ϕ is the thermal neutron fluence averaged over the volume of the ampule. Likewise, the net production rate for ^{196}Au is

$$\frac{dN_2}{dt} = K_1 N_{Au}\sigma_2\phi - \lambda_2 N_2 \quad , \tag{2}$$

where K_1 is the ratio of neutron fluence averaged over the length of gold wire to that averaged over the volume of lithium hydride (see Appendix B for this calculation); σ_2 is the thermal capture cross section of gold; and λ_2 is the decay constant of ^{196}Au. The solutions of these equations for an irradiation starting at $t = 0$ and ending at $t = t_e$ are

$$N_1(t_e) = N_{Li\text{-}6}\sigma_1[1 - \exp(-\lambda_1 t_e)]\phi/\lambda_1 \tag{3}$$

$$N_2(t_e) = K_1 N_{Au}\sigma_2[1 - \exp(-\lambda_2 t_e)]\phi/\lambda_2 \quad , \tag{4}$$

and these give

$$N_1(t_e) = N_2(t_e)\,\frac{N_{Li\text{-}6}\sigma_1\lambda_2}{N_{Au}\sigma_2\lambda_1}\,\frac{1 - \exp(-\lambda_1 t_e)}{1 - \exp(-\lambda_2 t_e)} \quad . \tag{5}$$

We determined $N_2(t_e)$, the number of ^{196}Au atoms at the end of the irradiation, by counting the 412-keV gamma rays with a Ge(Li) detector of efficiency ϵ. The number of ^{196}Au disintegrations per second in the interval Δt starting at elapsed time t_i after the

end of the reactor irradiation was determined from D, the number of 412-keV gamma rays detected, using the relation

$$E(t,\Delta t) = \frac{D}{T\epsilon\beta K_2} \quad , \tag{6}$$

where

(1) T is the measured transmission of the 412-keV gamma rays through the LiH sample and quartz wall;
(2) the constant β is a combination of the branching ratio and internal conversion coefficient in the decay of ^{196}Au; there are β 412-keV gamma rays per disintegration;
(3) K_2 is a coefficient that relates to the size of the gold wire used to measure neutron fluence (some neutrons entering the gold wire and gamma rays leaving the wire are absorbed).

In Appendix C we calculate K_2, the ratio of the fraction of gamma rays escaping the gold to the limiting value for an infinitely thin wire. Now

$$E(t_1,\Delta t) = N_2(t_e)\exp(-\lambda_2 t_1)[1 - \exp(-\lambda_2\Delta t)] \quad , \tag{7}$$

where we have accounted for ^{196}Au decay during elapsed time t_1 starting at time t_e and also for decay during the counting interval Δt. From Eqs. (6) and (7),

$$N_2(t_e) = \frac{D\exp(\lambda_2 t_1)}{T\epsilon\beta K_2[1 - \exp(-\lambda_2\Delta t)]} \quad , \tag{8}$$

and substituting for N_2 [Eq. (5)] we get for the number of tritium atoms formed in terms of the number of 412-keV gamma rays detected,

$$N_1 = \frac{N_{Li\text{-}6}\sigma_1\lambda_2[1 - \exp(-\lambda_1 t_e)]}{N_{Au}\sigma_2\lambda_1[1 - \exp(-\lambda_2 t_e)]} \cdot \frac{D\exp(\lambda_2 t_1)}{T\epsilon\beta K_1 K_2[1 - \exp(-\lambda_2\Delta t)]} \quad . \tag{9}$$

The mass of lithium per gram of LiH, g, was determined by Union Carbide's analysis of the material. The numbers $N_{Li\text{-}6}$ and N_{Au} of lithium and gold atoms are given by

$$N_{Li\text{-}6} = \frac{A}{A_{Li}} g m_1 f \tag{10}$$

and

$$N_{Au} = \frac{A}{A_{Au}} m_2 \quad , \tag{11}$$

where A_{Li} and A_{Au} are the atomic weights (for the isotopic mixtures as used) of the lithium and gold, A is Avogadro's number, and f is the isotopic abundance of ^{6}Li. The number of tritons formed per unit mass of LiH is then

$$\frac{N_1}{m_1} = \frac{A_{Au}}{A_{Li}} \cdot \frac{\sigma_1\lambda_2 g}{\sigma_2\lambda_1 m_2} \cdot \frac{fD\exp(\lambda_2 t_1)}{T\epsilon\beta K_1 K_2} \cdot \frac{1 - \exp(-\lambda_1 t_e)}{[1 - \exp(-\lambda_2 t_e)][1 - \exp(-\lambda_2\Delta t)]} \quad . \tag{12}$$

To compare calculated and measured tritium counting rates, we determined the decay rate per unit mass of LiH:

$$\frac{N_1\lambda_1}{m_1} = \frac{A_{Au}\sigma_1\lambda_2 g f[1 - \exp(-\lambda_1 t_e)]\, D\exp(\lambda_2 t_1)}{A_{Li}\sigma_2 m_2[1 - \exp(-\lambda_2 t_e)][1 - \exp(-\lambda_2\Delta t)]T\epsilon\beta K_1 K_2} \quad . \tag{13}$$

The constants appearing in Eqs. (12) and (13) have the values given below.

Constant	Value	Reference
A_{Au}	196.97	*CRC Handbook of Chemistry and Physics*, 58th ed.
A_{Li}	7.01506	(calculated)
σ_1	936 ± 4 b	8
σ_2	98.8 ± 0.3 b	9
λ_1	$1.7781 \times 10^{-6}\,s^{-1}$	10
λ_2	$2.976 \times 10^{-6}\,s^{-1}$	11
g	0.87075	Union Carbide
T	0.9447 (large ampules)	(measured)
	0.9710 (small ampules)	(measured)
ϵ	3.9811×10^{-6}	(measured)
β	0.9547	12
f	9.42×10^{-6}	Union Carbide and LASL analyses
K_1	1.005 (small ampules)	Appendix B
	1.013 (large ampules)	Appendix B
K_2	0.9690	Appendix C

Table IV, which gives the predicted [from Eq. (13)] and the measured tritium activities for the lithium hydride samples irradiated by thermal neutrons, shows that predicted-to-calculated ratios have values characteristic of the size of the sample. Table V summarizes this dependence and shows also the ratios of predicted and measured volumes of evolved gas. The fact that these have similar systematic variations suggests that most of the systematic error in Teledyne's tritium measurement is characteristic of the process of gas evolution and conversion to water. Using the thermal fluence tritium-production measurements to establish standards, we normalized the tritium determination results from Teledyne for the small and large samples by the divisors (from Table V) 1.103 and 1.058, respectively. If we note that Teledyne's quoted systematic error for the entire process was 5%, we find these normalizations quite plausible.

We adduce an additional piece of evidence that supports the assumption that the systematic error in the Teledyne measurement is characteristic of the sample processing. Teledyne measured the tritium decay in sample 305, which contained 0.1594 g of LiH, with 0.1 at.% ^{6}Li. This was one of the test samples irradiated in thermal neutron flux. This sample was converted to gas and additional hydrogen carrier gas was added in a manner typical of all small ampules. The total volume was then converted to water; an aliquot of this sample was converted back to hydrogen and counted in a gas proportional counter with a resulting activity of 347.15 dis·s^{-1}· (g H_2O)$^{-1}$ as of 24 June 1976. Another aliquot of the water from this sample was certified

TABLE IV

TRITIUM ACTIVITY INDUCED BY THERMAL NEUTRON IRRADIATION

Sample No.	Mass ^{7}LiH, m_1 (g)	Tritium Counting Rate,* $m_1^{-1} \cdot dN_1/dt$ [10^8 counts·s^{-1}·(g LiH)$^{-1}$] Predicted	Measured	Ratio Measured/ Predicted
302	0.1384	2.205	2.362	1.071
305	0.1594	2.165	2.528	1.168
307	0.1655	2.135	2.362	1.106
309	0.1598	2.067	2.212	1.070
312	0.1496	2.271	2.528	1.113
313	0.1682	2.150	2.345	1.091
				av = 1.103 ± 0.015
315	0.8789	2.223	2.428	1.092
319	0.9269	2.180	2.262	1.038
321	1.0486	2.319	2.462	1.062
326	0.9291	2.117	2.191	1.035
328	0.9232	2.283	2.428	1.064
				av = 1.058 ± 0.010

*As measured by Teledyne and as predicted from the gold activation. Fractional ^{6}Li abundance was 9.42 x 10^{-4}. Reference time was 1200 MST, 26 February 1976.

TABLE V

RATIOS OF MEASURED-TO-PREDICTED VALUES FOR VOLUMES AND ACTIVITIES OF EVOLVED GASES

Sample Size	Average Ratio of Volume H_2[a]	Measured-to-Predicted Tritium Activity[b]
Small	1.0257 ± 0.005	1.103 ± 0.015
Large	0.9519 ± 0.015	1.058 ± 0.010

[a]Predicted values were obtained from LiH mass and the Union Carbide reported value for the number of grams of H_2 per gram of LiH.

[b]Predicted values are derived from thermal activations (see Table IV).

by NBS to have an activity of 315.5 ± 6 dis·s^{-1}·(g H_2O)$^{-1}$ as of 24 June 1976. (The uncertainty of 6 $s^{-1}\cdot g^{-1}$ is the linear sum of 1.3, the random error at 99% confidence level, and 4.7, the linear sum of conceivable systematic errors.) The ratio of these two measurements is 1.1003, consistent with the correction factor (see Table IV) determined by the gold-monitored thermal activations of the small samples. We have already seen (Table II) that Teledyne and NBS determinations of tritium activities in two fractions of a sample of tritiated water agree within 1.5% (which is expected because both determinations are referred to as the same standard sample) so the systematic error is probably characteristic of Teledyne's gas handling system.

IV. TRITIUM-PRODUCTION RESULTS

The neutron production from the T(d,n) reaction in the target inside the ^{6}LiD assembly was monitored by counting the alpha particles from the target in a small solid angle at 135° with respect to the deuteron beam direction. The total number of source neutrons produced was (9.42 ± 0.28) x 10^{15}. Additional data on the total number of neutrons and the change in their energy spectrum as they were transported through the ^{6}LiD assembly were acquired by the LASL Radiochemistry Group, CNC-11, through the use of various activation foils. These results[18] appear in Part II; those obtained at the inner surface provide a measure of the 14-MeV neutron flux and are compatible with the alpha-particle monitor data.

The results of Teledyne's analyses of the samples of lithium hydride are given in Table VI. In tabulating the Teledyne counting data, we subtracted from their reported number of counts per gram of lithium hydride the same quantity for unexposed samples. The backgrounds measured in irradiated ampules containing only helium were negligibly small. We applied an additional correction because Teledyne used 12.26 yr for the half-life of tritium in determining the activity as of 26 Feburary 1976 from an NBS standard dated 3 September 1961. The apparent best value for the tritium half-life is 12.35 yr (Ref. 10), implying that Teledyne's counting data should be multiplied by 1.006.

The results for both lithium isotopes are plotted in Fig. 9, along with the results of measurements by Wyman.[1] Although his measurements were made in an assembly of the deuteride of natural lithium, his results are nearly the same as those in this experiment.

The fractional standard deviation for data listed in Table VI is 6%.

To evaluate the systematic errors in these tritium-production measurements, we assumed that the standard deviations in the normalizations (those found for the measured-calculated ratios in Table V—1.5 and 1.0% for small and large ampules, respectively) are also systematic errors in these determinations. The standard used to determine the counter efficiency for the 412-keV gamma rays for gold had an error quoted by the Laboratoire de Métrologie des Rayonnements Ionisants as ±2% at 99% confidence level. We checked this source against a separate standard, used by radiochemists at LASL, whose uncertainty was also quoted as ±2% at the 99% level. The two standards agreed to within 2%, and we used an average of the two, assigning a 2% systematic error. The standard deviation of 3% in the neutron-source strength also appears as a systematic error. We used the linear sums of the errors to obtain total systematic errors of 6.5 and 6% for small and large samples, respectively.

TABLE VI

RESULTS OF TRITIUM-PRODUCTION MEASUREMENTS

Li Isotope	Sample No.	Mass LiH[a] (g)	Location (see Fig. 4) r (mm)	Location (see Fig. 4) ω[b] (deg)	Tritium Decay Rate[c] [s⁻¹·(g LiH)⁻¹] Teledyne (2/26/76)	Teledyne Net[d] (2/26/76)	Normalized and Corrected[e] (3/27/76)	f(r)[f] [10⁻²⁴ atoms·mm²·(Li atom)⁻¹·(source neutron)⁻¹]
6	136	1.107	299.5	20	33.0		31.23	24.66
	137	1.0544	299.5	−20	36.67		34.71	27.41
	145	1.0429	299.5	135	45.0		42.59	33.63
	138	0.9464	201.5	−15	228.3		216.1	77.24
	139	1.0213	201.5	−35	240.0		227.2	81.21
	140	1.0584	201.5	−145	240.0		227.2	81.21
	141	0.9983	127.5	−30	601.7		569.5	81.50
	142	0.9831	127.5	−135	583.3		552.1	79.01
	143	1.0939	125.5	30	668.3		632.5	87.70
	104	0.1409	77.64	−55	1067		969	51.42
	111	0.1218	76.66	40	1088		988	51.13
	106	0.1432	51.2	−45	1717		1559	35.99
	110	0.1367	49.5	50	1683		1528	32.97
7	183	0.9054	299.5	−20	17.17	13.39	12.67	11.36
	186	0.9128	299.5	120	17.0	13.22	12.51	11.21
	147	0.8432	201.5	−125	52.67	47.89	45.33	18.39
	173	0.9343	199.5	35	59.33	54.55	51.63	20.53
	149	0.7892	127.5	−30	168.33	164.6	155.8	25.31
	171	0.9086	125.5	30	166.7	162.9	154.1	25.03
	172	0.8788	125.5	135	166.7	162.9	154.1	25.03
	101	0.1485	77.68	−40	570.0	566.2	514.0	30.96
	114	0.1211	75.66	55	566.7	562.9	511.0	29.23
	103	0.1340	49.5	−50	1353	1349	1224	29.97
	109	0.1303	51.5	45	1342	1338	1215	32.20

[a]Isotopic abundances in the test samples were: ^{6}Li, 95.5034%; ^{7}Li, 99.9058%. Molecular weights used were ^{6}LiH, 7.068; ^{7}LiH, 8.023.

[b]Positive angles are below the parting plane in Fig. 4; negative angles are above.

[c]Counting rate of evolved tritium.

[d]Tritium activities in ^{7}LiH samples were corrected for a background measured in unirradiated samples of 3.78 ± 0.52 s^{-1} · (g LiH)$^{-1}$ (see Table III); ^{6}LiH samples had negligible background.

[e]Teledyne counting data were corrected because they were based on a tritium half-life of 12.26 yr instead of the presently accepted 12.35 yr; this affects the NBS standard used (dated 9/3/61).

[f]The specific tritium production, f(r), (equals $4\pi r^2$ times number of tritons formed per atom of lithium for one source neutron).

ACKNOWLEDGMENTS

We are grateful to the machine operators in LASL Group R-2 for operation of the C-W machine; to James J. Bramble for design of the ^{6}LiD assembly; and to the staff at Union Carbide Corporation, Oak Ridge, TN 37830, for fabrication of the ^{6}LiD assembly and preparation of the LiH-filled ampules. We especially thank J. David Martin at Teledyne Isotopes, Westwood, NJ 07675, whose expertise in tritium measurements made this project possible.

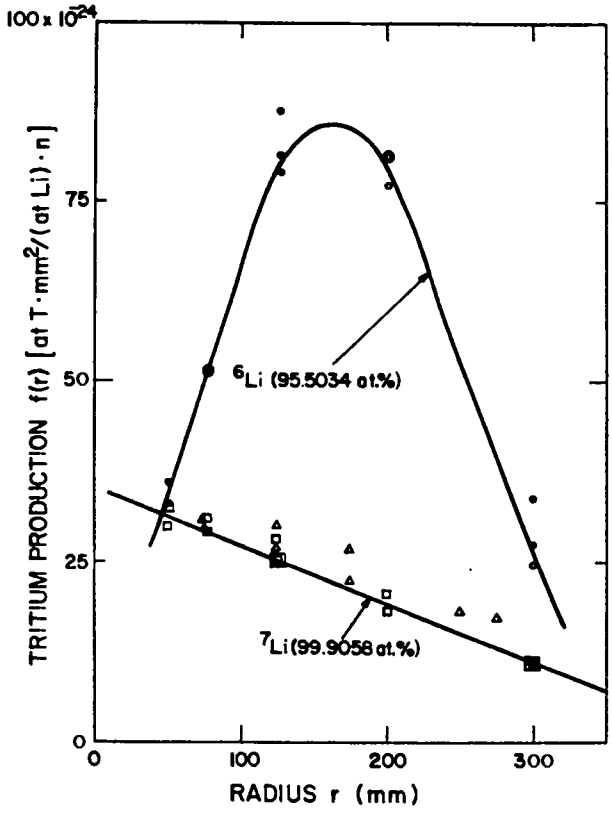

Fig. 9.
Tritium production in a sphere of ⁶LiD plotted as f(r) = 4πr² times the number of tritons per atom of lithium for one 14-MeV neutron at the center of the assembly. The triangles are measurements by Wyman[1] of tritium production in ⁷Li metal embedded in a sphere of LiD. The circles are our ⁶Li production data; the squares, ⁷Li data. The curves are drawn to guide the eye.

APPENDIX A

TRITIUM DECAY RATES IN SAMPLES OF UNIRRADIATED ⁷LiD

Tritium decay rates in samples of ⁷LiD prepared by Union Carbide Corporation are listed in Table A-I.

TABLE A-I

BACKGROUNDS IN ⁷LiD SAMPLES[a]

Sample No.	Mass LiD (g)	Activity [10^4 counts·s^{-1}·(g LiD)$^{-1}$]
65	0.1733	1.638
69	0.2028	1.138
107	1.1078	1.317
108	1.1397	1.317
109	1.0285	1.299
110	0.9681	1.242
111	1.0162	1.221
		av = 1.310 ± 0.060

[a]As of 1 July 1975. The atomic abundance of ⁶Li was 1.047×10^{-4}.

APPENDIX B

CALCULATION OF VOLUME-AVERAGED NEUTRON FLUENCE

To find a value for the thermal neutron fluence averaged over the volume of lithium hydride in a quartz ampule, we must take account of the attenuation of flux as it passes through the lithium hydride itself. These types of calculations have been done for purely absorbing media by Case, de Hoffmann, and Placzek[14] for several different geometries. For a sphere of radius a immersed in an isotropic bath of monoenergetic neutrons, the average flux throughout the volume relative to that far away is given by

$$P_0 = 1 - \frac{3}{4}\frac{a}{\ell} \qquad \left(\frac{a}{\ell} \ll 1\right) ,$$

where ℓ is the absorption mean free path. For a sphere of lithium hydride [(9.42×10^{-2})% ^{6}Li] with a = 8.0 mm and ℓ = 257.9 mm, $a/\ell = 0.0310$ and $P_0 = 0.9767$. Thus the fluence averaged over the sphere is only a few per cent different from the fluence far away. This difference is an upper limit of the correction necessary because the gold was distributed along a diameter and not throughout the volume.

If $\phi(r)$ represents the radial distribution of neutrons in the sphere, then the average fluence interacting with the lithium hydride is given by

$$\bar{\phi}_v = 3/a^3 \int_0^a \phi(r) r^2 \, dr ,$$

and the fluence averaged along a radius is given by

$$\bar{\phi}_r = 1/a \int_0^a \phi(r) \, dr .$$

With the gold wire positioned along a diameter of the ampule, we determined $\bar{\phi}_r$ by counting the number of 412-keV gamma rays.

We used the code DTF-IV (Ref. 15) to estimate $\phi_r(r)$ in one-group S_n calculations with n = 8, assuming isotropic scattering in the center of mass. Calculations were performed using both purely absorbing media and with several different estimates of the scattering cross section for lithium hydride molecules. Neutron interactions in the quartz ampules were also included in the calculations. We calculate that the ratio of the averaged fluxes,

$$K_1 = \frac{\bar{\phi}_r}{\bar{\phi}_v} ,$$

is 1.005 ± 0.002 for the small ampules and 1.013 ± 0.005 for the large ones. This relation was used to compute the amount of tritium produced in the two different size ampules.

APPENDIX C

NEUTRON AND GAMMA-RAY ABSORPTION IN GOLD WIRE

A 0.05-mm-diam gold wire in the form of a helix was positioned along the diameter of the ampule to measure the thermal neutron fluence within the test samples of LiH. Gold has a sufficiently large neutron capture cross section that the interior of the wire is in a fluence lower than that at the outside of the wire. Furthermore, some of the 412-keV gamma rays originating in the interior of the wire fail to escape. These effects are smaller than 5%, and we calculated the correction for them.

We assume that the pitch of the gold helix is great enough—perhaps 50 wire diameters—that we can make the calculation for an infinite straight wire. The calculations for neutrons entering and gamma rays leaving are identical. We refer to the calculation of average fluence by K. M. Case, F. de Hoffmann, G. Placzek[14] for a purely absorbing medium. Their calculation is appropriate for gold, which has a cross section for absorption 10 times greater than that for scattering. For radii small compared to the mean free path, they find for the escape or entrance probability,

$$P_0 = 1 - \frac{4}{3}\frac{a}{\ell} + \frac{1}{2}\left(\frac{a}{\ell}\right)^2 \log\left(\frac{2\ell}{a}\right) + \frac{1}{2}\left(\frac{a}{\ell}\right)^2 \left(\frac{5}{4} - \gamma\right) ,$$

where Euler's constant $\gamma = 0.577216$.

For gold the capture cross section of 98.8 b gives a mean free path ℓ_1 of 1.715 mm. For radius a = 0.0254 mm, $a/\ell_1 = 0.01481$ and, from the above equation, $P_0 = 0.9809$.

For the gold gamma ray, $\sigma_{abs} = 62$ b, which gives a mean free path $\ell_2 = 2.733$ mm. Then $a/\ell_2 = 0.00929$ and $P_0 = 0.9879$.

The product of the entrance and escape probabilities is the constant, $K_2 = 0.9690$, used in Eq. (6).

REFERENCES

1. Marvin E. Wyman, "An Integral Experiment to Measure the Tritium Production from ^{7}Li by 14-MeV Neutrons in a Lithium Deuteride Sphere," Los Alamos Scientific Laboratory report LA-2234, Rev. (November 1972).

2. R. Herzing, L. Kuijpers, P. Cloth, D. Filges, R. Hecker, and N. Kirch, "Experimental and Theoretical Investigations of Tritium Production in a Controlled Thermonuclear Reactor Blanket Model," Nucl. Sci. Eng. **60**, 169 (1976).

3. Lambert J. M. Kuijpers, "Experimental Model Studies for a Fusion Reactor Blanket," thesis, Technische Hogeschool, Eindhoven, Netherlands (1976).

4. H. Bachmann, V. Fritscher, F. W. Kappler, D. Rusch, H. Werle, and H. W. Wiese, "Neutron Spectra and Tritium Production Measurements in a Lithium Sphere to Check Fusion Reactor Blanket Calculations," Nucl. Sci. Eng. **67**, 74 (1978).

5. D. W. Muir and M. Wyman, "Neutronic Analyses of a Tritium Production Integral Experiment," Tex. Symp. Technol. CTR Exp. November 20-22, 1972, Austin, Texas (1972).

6. S. M. Qaim, R. Wölfle, and G. Stöcklin, "Nuclear Data for Fusion Reactors," ATOMKI Kozl. 18, 335 (1976)

7. S. M. Qaim, R. Wölfle, and G. Stöcklin, "Radiochemical Methods in the Determination of Nuclear Data for Fusion Reactor Technology," J. Radioanal. Chem. **30**, 35 (1976).

8. Norman Holden, National Neutron Cross Section Center, Brookhaven National Laboratory, Upton, NY 11973, private communication, 1976.

9. S. F. Mughabghab and D. I. Garber, "Neutron Cross Sections, Resonance Parameters," Brookhaven National Laboratory report BNL-325 (1973) Vol. 1, p. 79.

10. M. J. Martin and P. H. Blichert-Toft, "Radioactive Atoms," Nucl. Data Tables 8, 14 (1970).

11. M. J. Martin and P. H. Blichert-Toft, "Radioactive Atoms," Nucl. Data Tables 8, 153 (1970).

12. Ronald L. Auble, Nuclear Data Group, Oak Ridge National Laboratory, Oak Ridge, TN 37830, private communication, 1976.

13. Donald W. Barr, Los Alamos Scientific Laboratory Group CNC-11, private communication, 1976.

14. K. M. Case, F. de Hoffmann, and G. Placzek, "Introduction to the Theory of Neutron Diffusion," (Los Alamos Scientific Laboratory, Los Alamos, NM 87545, 1953), Vol. I.

15. Kaye D. Lathrop, "DTF-IV, a FORTRAN-IV Program for Solving the Multigroup Transport Equation with Anisotropic Scattering," Los Alamos Scientific Laboratory report LA-3373 (November 1965).

PART II

CALCULATIONS OF TRITIUM PRODUCTION AND RADIOCHEMICAL ACTIVATION IN A SPHERE OF ^{6}LiD IRRADIATED BY 14-MeV NEUTRONS

by

Jon M. Wallace

ABSTRACT

The specific production of tritium in ^{6}LiH and ^{7}LiH embedded ampules and the activation of radiochemical detector foils of ^{45}Sc, ^{89}Y, ^{90}Zr, ^{169}Tm, ^{191}Ir$_{.373}$ ^{193}Ir$_{.627}$, ^{197}Au, ^{236}U, and ^{238}U placed at various positions in a 600-mm-diam ^{6}LiD sphere irradiated by a central source of 14-MeV neutrons have been calculated and compared with experimental data. One- and three-dimensional Monte Carlo and S_n neutron-transport calculations were performed. The most reliable (three-dimensional Monte Carlo) calculation generally agrees with both the tritium-production and the radiochemical-activation data. The existing discrepancies between calculation and experiment appear largely attributable to uncertainties in some tritium-production and radiochemical-activation cross sections.

I. INTRODUCTION

We present the results of neutron-transport calculations in a 600-mm-diam sphere of ^{6}LiD irradiated by a central 14-MeV neutron source. Tritium production from lithium in embedded ^{6}LiH and ^{7}LiH ampules and the neutron-induced activation of radiochemical detector foils placed at various positions in the sphere were obtained and compared with experimental data. The ^{6}LiD sphere, the neutron source, and the tritium-production measurements have been described in detail in Part I of this report. Additional diagnostic information was obtained from six radiochemical foil packets placed at the interfaces of the concentric ^{6}LiD spherical assembly. The foil materials were ^{45}Sc, ^{89}Y, ^{90}Zr, ^{169}Tm, ^{191}Ir$_{.373}$ ^{193}Ir$_{.627}$, ^{197}Au, ^{236}U, and ^{238}U. The foils were analyzed by radiochemical methods after the irradiation.

The comparison of our calculations with the integral experiment provides a simultaneous test of the neutron-transport codes, the neutron cross-section data relevant to transport through ^{6}LiD, the tritium-production cross-section data, and the radiochemical-activation cross-section data.

II. CALCULATIONS

Four different calculations of this experiment will be discussed. They vary in reliability, and their intercomparison is instructive because it points out the shortcomings of the less accurate calculations. Each calculation consisted of two parts: (1) a neutron-transport computation to produce fluences, that is time-integrated fluxes, at various detector positions, and (2) an evaluation of the radiochemical-activation integrals and, for Calculations I-III, the tritium-production integrals for comparison with the experimental values. In Calculation IV, the tritium production was obtained directly in the neutron-transport computation. The ^{6}Li and ^{7}Li

cross-section data used in both the transport and tritium-production computations were ENDF/B-III. The 1967 United Kingdom/LASL evaluation of the deuterium cross sections was employed in the transport computation. The radiochemical-activation cross sections used were from the LASL TD-Division Dosimetry Library.* The (n,f) and (n,γ) cross sections in this library were normalized[1] using BIG 10** data. There is a 3% normalization uncertainty in our results that is due to the uncertainty in the number of 14-MeV source neutrons, as described in Part I of this report. The calculations will now be discussed in order of increasing reliability.

A. Calculation I—1D, 11-Group, S_4,P_1

In this calculation the neutron fluences at the required radial distances from the source were computed using a one-dimensional neutron transport code with 11-group, S_4,P_1 neutron transport. The group structure is given in Table I. The source neutrons were distributed between 13.5 and 17.0 MeV according to an appropriate weighting function. The radiochemical-activation and tritium-production integrals were computed with cross sections collapsed into the 11-group structure using the same weighting function.

B. Calculation II—1D, 21-Group, S_8,P_1

This calculation is similar to Calculation I, except smaller energy and angle bins are used in a 21-group, S_8P_1 transport scheme. The energy group structure is given in Table II. In this computation, group 1 is empty. The source neutrons were distributed between 13.5 and 15.0 MeV according to the weighting function used in Calculation I. As in Calculation I, this weighting function was also used to collapse the radiochemical-activation and tritium-production cross sections into the 21-group structure.

TABLE I

ENERGY GROUP STRUCTURE FOR CALCULATION I

Group Number	E_{Lower} (MeV)
1	13.5
2	10.0
3	7.79
4	3.68
5	2.232
6	0.500
7	0.184
8	0.0248
9	0.00335
10	0.000167
11	0.139×10^{-6}
	$E_{Max} = 17.0$

C. Calculation III—1D, Monte Carlo

In this calculation the neutron fluences at the required radial distances from the source were computed using the three-dimensional Monte Carlo neutron-transport code MCN.[2,3] A one-dimensional mockup of the spherical assembly, similar to that in Calculations I and II, was used. The fluences, which were surface integrated, were binned into a 75-group structure (Table III). The point-source neutrons were distributed isotropically with energy 14.1 MeV. Radiochemical-activation and tritium-production integrals were calculated using precollapsed cross sections and the 75-group histogram fluences. The fluences in the high-energy range relevant to the (n,2n) activations were increased by 2% to simulate the effect of the observed source anisotropy in the direction of the radiochemical detectors. This is our most reliable one-dimensional calculation. The relevant geometric parameters for Calculations I-III are given in Table IV.

*The Sc(n,γ) cross sections are based on ENDF/B-IV, Dosimetry Library. The Y(n,γ) cross sections were taken from an evaluation by E. D. Arthur in "Applied Nuclear Data Research and Development," LASL report LA-6971-PR (September 1977) (compiled by C. I. Baxman and P. G. Young), p. 3. The Tm(n,γ) cross sections are from a private file of J. S. Hendricks. The (n,2n) cross sections, except for ^{238}U, were taken from evaluations based on data in B. P. Bayhurst, Phys. Rev. C 12, 451 (1975). All other activation cross sections were based on ENDL (Livermore Evaluated Nuclear Data) 4/76.

**BIG 10 is a critical assembly at LASL.

TABLE II

ENERGY GROUP STRUCTURE FOR CALCULATION II

Group Number	E_{Lower} (MeV)
1	15.0
2	13.5
3	12.0
4	10.0
5	7.79
6	6.07
7	3.68
8	2.865
9	2.232
10	1.783
11	1.353
12	0.823
13	0.500
14	0.303
15	0.184
16	0.0676
17	0.0248
18	0.00912
19	0.00335
20	0.000167
21	0.139×10^{-6}

$E_{Max} = 17.0$

TABLE III

ENERGY GROUP BOUNDARIES FOR BINNING IN CALCULATIONS III AND IV

15.22 MeV[a]		12.33	6.50	0.500
15.12[a]		12.16	6.28	0.400
15.00[a]		12.00	6.07	0.303
14.87[a]		11.75	5.78	0.244
14.75[a]		11.50	5.50	0.184
14.62[a]		11.25	5.25	0.125
14.50[a]		11.00	5.00	0.0676
14.37[a]		10.75	4.75	0.0460
14.25[a]	14.11[b]	10.50	4.50	0.0248
14.12[a]	14.05[b]	10.25	4.09	0.0170
14.00		10.00	3.68	0.00912
13.87		9.75	3.27	0.00600
13.75		9.50	2.865	0.00335
13.62		9.25	2.55	0.001235
13.50		9.00	2.232	0.000454
13.37		8.75	2.000	0.000167
13.25		8.50	1.738	0.0000614
13.12		8.15	1.550	0.0000
13.00		7.79	1.353	
12.83		7.40	1.090	
12.67		7.00	0.823	
12.50		6.75	0.660	

[a]Energy boundaries for Calculation IV.

[b]Energy boundaries for Calculation III.

TABLE IV

GEOMETRICAL DATA FOR CALCULATIONS I-III

Outside Radius (mm)	Material	Density (g/cm^3)
22.2	Vacuum	0.0
50.0	$^6Li_{.9659}$ $^7Li_{.0441}$ $D_{1.0}$	0.753
51.0	Vacuum	0.0
76.15	$^6Li_{.9559}$ $^7Li_{.0441}$ D	0.753
77.15	Vacuum	0.0
126.0	$^6Li_{.9569}$ $^7Li_{.0441}$ D	0.753
127.0	Vacuum	0.0
200.0	$^6Li_{.9568}$ $^7Li_{.0432}$ D	0.751
201.0	Vacuum	0.0
300.0	$^6Li_{.9568}$ $^7Li_{.0462}$ D	0.755

D. Calculation IV—3D, Monte Carlo

The neutron fluences in this calculation also were obtained using MCN. The calculation incorporated a simplified three-dimensional mockup of the spherical assembly, including small spherical ^{6}LiH and ^{7}LiH regions to simulate the tritium collection ampules. The geometric data are given in Table V. The geometry is illustrated in Fig. 1. Tritium production was calculated on-line by the neutron-transport code. Neutron fluences for the radiochemical-activation integrals were tallied at the points where the detectors were located for neutron energies >7.40 MeV. Surface integrated fluences, as in the one-dimensional calculations, were used for energies E < 7.40 MeV. This hybrid treatment was employed because the MCN point-fluence tally is very time consuming. The tally should not be necessary at lower energies because the multiple-scattering process, which produces the lower energy component of the neutron spectra, tends to produce an isotropic distribution as the neutrons are downscattered. For this calculation, the fluences were binned into an 83-group structure (Table III), which consisted essentially of the group structure of Calculation III with eight additional groups at the upper energy end. The calculation employed an anisotropic energy-angle correlated source occupying a spherical volume, which closely simulated the experimental source (see Fig. 3 of Part I of this report). The energy-angle correlation is that produced by a 240-keV deuteron beam on a tritium target.* The radiochemical activations were obtained just as in Calculation III, using the histogram fluences. Of the four calculations, this one is the

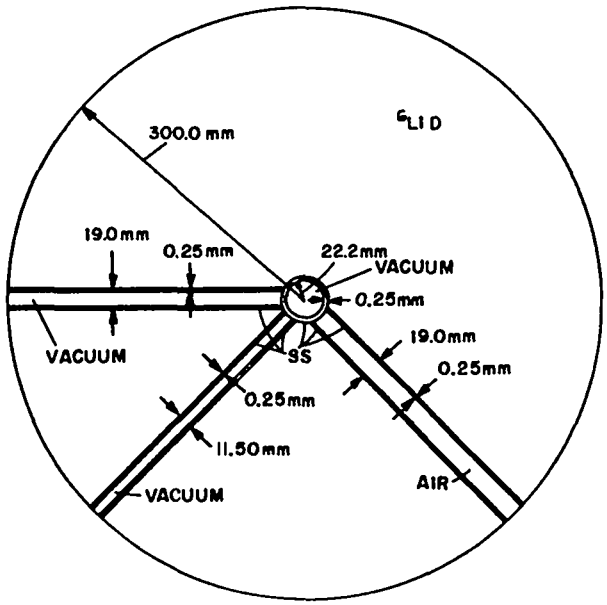

Fig. 1.
The geometry of the ^{6}LiD sphere used in Calculation IV. The small embedded LiH spheres are not shown, but are located at the positions illustrated in Fig. 4 of Part I of this report. The radii of the LiH spheres in the calculation are in some cases larger than the radii of the ampules used in the experiment (Table V).

TABLE V

GEOMETRICAL DATA FOR CALCULATION IV[a]

Material	Density (g/cm^3)
^{6}Li$_{.9564}$ ^{7}Li$_{.0436}$ D	0.7425
Stainless steel (SS)	9.03
LiH	0.300

Distance of Center From Source (mm)	Radius of LiH Spheres	
	Experiment (mm)	Calculation (mm)
50.5	5.0	5.0
76.65	5.0	6.0 ^{6}LiH
		5.5 ^{7}LiH
126.5	9.0	9.0
200.5	9.0	9.0 ^{6}LiH
		12.0 ^{7}LiH
300.0	9.0	15.3

[a]Source volume: spherical region of radius 2.0 mm.

*For this calculation, this correlation is identical to that for the 300-keV beam actually used in the experiment.

most precise simulation of the experiment. Comparison of the results of this calculation with the experimental data provides the best test of how well we understand the processes under consideration.

III. TRITIUM PRODUCTION

The experimental tritium-production results at each radius have been averaged for comparison with the calculations. This average is the proper comparison for Calculations I-III, which are spherically symmetric, and provides better statistics for comparison with Calculation IV. In addition, the tritium-production results are compared ampule by ampule with the results of Calculation IV.

All comparisons are made in terms of the ratio of the experimental results to the calculated results. The quoted uncertainties for this ratio are from the experimental uncertainties only.

A. Tritium Production From ^{7}Li

The material contained in the ampules was $^7Li_{.999058}$ $^6Li_{.000942}$ H. So the quantity observed was

$$A_i^{Li-7} = 4\pi r^2\left[0.999058\int \phi_i(E)\sigma_{Li-7}(E)\,dE + 0.000942\int \phi_i(E)\sigma_{Li-6}(E)\,dE\right],$$

where σ_{Li-7} is the reaction cross section for ^{7}Li(n,n'α) and σ_{Li-6} is the reaction cross section for ^{6}Li(n,α).

Here ϕ_i is the neutron fluence spatially integrated over the ampule volume. The amount of tritium produced from ^{6}Li is never more than 0.3% of the total. The ^{7}Li tritium-production reaction threshold is at 2.8 MeV; thus these data probe neutron transport only in the energy range above this threshold.

The results of the calculations are presented in Tables VI and VII and shown in Fig. 2. The various calculations differ from each other by as much as ~25% at the 300.0-mm radius (at the outside of the LiD sphere) with typically 10% differences at the other positions. All calculations give overpredictions at the inner three positions. Calculation IV gives the best overall agreement with experiment, the discrepancies being generally smaller at positions further away from the source. These results are similar to those of a recent analysis of the Wyman experiment.[4-6] In Secs. IV.A and IV.B we discuss (n,2n) and (n,f) activations of ^{238}U, in which there is generally good agreement between calculation and experiment. The cross sections for these two reactions are qualitatively similar to the ^{7}Li tritium-production cross section and are thought to be relatively well known. Hence it is not unreasonable to attribute the ^{7}Li discrepancies to the tritium-production cross section used. A 15% reduction of the cross section in the 14-MeV region would bring

TABLE VI

RATIO OF OBSERVED-TO-CALCULATED TRITIUM PRODUCTION FROM ^{7}Li

Distance From Source (mm)	Average Experimental Result (10^{-24} atoms·mm^3/Li atom)	Calculation[a] I	II	III	IV
50.5	31.09	0.783	0.836	0.873	0.883
76.65	30.10	0.811	0.838	0.882	0.861
126.5	25.12	0.834	0.809	0.860	0.890
200.5	19.46	0.989	0.883	0.926	0.918
300.0	11.29	1.256	1.024	1.015	0.986

[a]Ratio of experiment to calculation.

TABLE VII

CALCULATION IV AND OBSERVED TRITIUM PRODUCTION FROM ^{7}Li

Sample No.	Distance From Source (mm)	Observation (10^{-24} atoms·mm^2/Li atom)	Calculation IV (10^{-24} atoms·mm^2/Li atom)
109	50.5	32.20	35.6
103		29.97	34.8
114	76.65	29.23	35.5
101		30.96	34.4
171	126.5	25.03	28.3
149		25.31	29.5
172		25.03	26.9
173	200.5	20.53	21.1
147		18.39	21.3
183	300.0	11.36	12.0
186		11.21	10.9

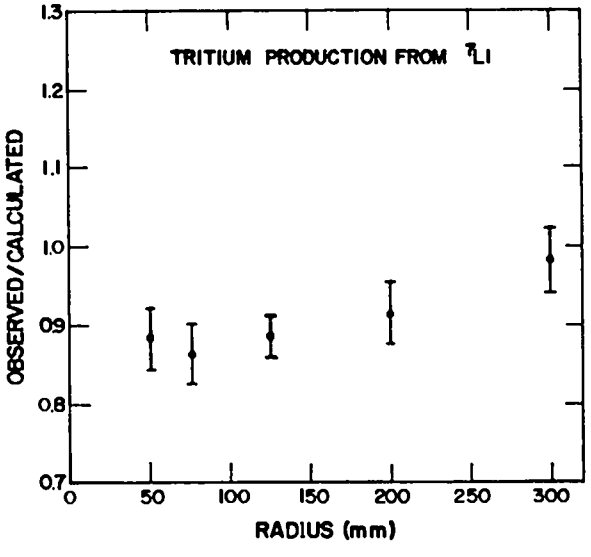

Fig. 2.
Ratio of observed-to-calculated tritium production from ^{7}Li vs radius. The error bars are from random experimental uncertainties only. There is an additional normalization uncertainty of ~3%.

the calculation into significantly better agreement with the experiment.

B. Tritium Production From ^{6}Li

The material contained in the ampules was $^7Li_{.044966}$ $^6Li_{.955034}$ H; so the observed quantity was

$$A_i^{Li-6} = 4\pi r^2\left[0.044966 \int \phi_i(E)\sigma_{Li-7}(E)\, dE + 0.955034 \int \phi_i(E)\sigma_{Li-6}(E)\, dE\right] .$$

The ^{7}Li contributes no more than ~5% of the tritium produced in these ampules, with the largest fractional contributions generally occurring in the ampules closest to the source. The cross section for tritium production from ^{6}Li is reasonably well known. It has a general decrease with energy, with a resonance superimposed at 240-keV neutron energy. Most of the tritium production arises from neutron energies around and below this resonance energy.

TABLE VIII

RATIO OF OBSERVED-TO-CALCULATED TRITIUM PRODUCTION FROM ^{6}Li

Distance From Source (mm)	Average Experimental Results (10^{-24} atoms·mm²/Li atom)	Calculation[a]			
		I	II	III	IV[b]
50.5	34.48	0.877	1.020	1.089	1.039
76.65	51.28	0.840	0.953	1.029	0.863
126.5	82.74	1.006	1.086	1.187	1.087
200.5	79.89	1.071	1.074	1.179	1.014
300.0	28.57	1.289	1.213	1.441	0.963

[a]Ratio of experiment to calculation.

[b]Ampule density ρ = 0.300 g/cm³.

TABLE IX

CALCULATION IV AND OBSERVED TRITIUM PRODUCTION FROM ^{6}Li

Sample No.	Distance From Source (mm)	Observation (10^{-24} atoms·mm²/Li atom)	Calculation IV (10^{-24} atoms·mm²/Li atom)
110	50.5	32.97	33.0
106		35.99	33.4
111	76.65	51.13	59.1
104		51.42	59.7
143	126.5	87.70	75.5
141		81.50	79.3
142		79.01	73.5
138	200.5	77.24	81.5
139		81.21	76.0
140		81.21	78.7
136	300.0	24.66	30.3
137		27.41	30.6
145		33.63	28.1

Resonance self-shielding is significant here, because strong contributions come from the region of the resulting dip in the neutron spectra. Comparison with the ^{6}Li tritium-production data provides a much more stringent test of our calculational capability than comparison with the ^{7}Li data.

The results of the various calculations are presented in Tables VIII and IX and shown graphically in Fig. 3. The various calculations differ from each other by 15 to 25%. As for ^{7}Li, Calculation IV gives the best overall agreement with experiment. An anomalously large discrepancy occurs at the radial source distance of 76.65 mm, for reasons unknown. The three-dimensional calculation gives a significantly different radial dependence of the

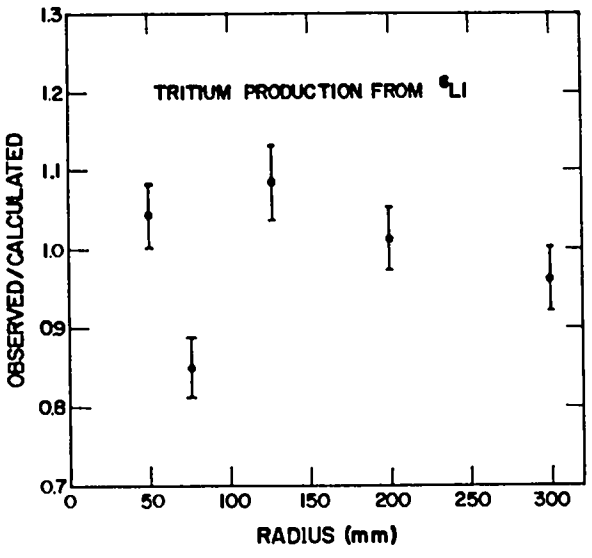

Fig. 3.
Ratio of observed-to-calculated tritium production from ^{6}Li vs radius. The error bars are from random experimental uncertainties only. There is an additional normalization uncertainty of ~3%.

tritium production at this point than do the one-dimensional calculations. At all other radii, Calculation IV is in rather good agreement with the experiment. Tritium production from ^{6}Li was quite sensitive to small changes in the device geometry, probably caused, at least partially, by resonance self-shielding. For example, there is a surprisingly large sensitivity just to changes in the density of the small LiH collection spheres. Changing the density from 0.30 to 0.50 g/cm^3 induces changes in the tritium production by as much as 10% in the larger LiH collection spheres. Given this high sensitivity together with the simplifications used in the Monte Carlo simulation of the experiment, we cannot reasonably expect much closer agreement between calculation and experiment than was obtained.

IV. RADIOCHEMICAL ACTIVATION

Three classes of activation reactions were considered: (n,2n), (n,f), and (n,γ). The (n,n') activation of ^{191}Ir was also observed. The targets were ^{45}Sc, ^{89}Y, ^{90}Zr, ^{169}Tm, ^{191}Ir$_{.375}$ ^{193}Ir$_{.627}$, ^{197}Au, ^{235}U, and ^{238}U. The foil packets were placed in the plane perpendicular to the horizontal deuteron beam and 60° up from the horizontal axis, $\phi = 60°$ and $\theta = 90°$ in the coordinate system of Part I. The foil distances from the source were 22.2, 50.0, 76.15, 126.0, 200.0, and 300.0 mm. The foils were sufficiently thin that they did not significantly effect the neutron flux in the ^{6}LiD assembly.

The observed quantities are

$$\int \phi_i(E)\sigma_j(E)\, dE \quad ,$$

where σ_j is the activation reaction cross section for reaction j and ϕ_i is the neutron fluence at the foil position i. The data for this part of the experiment[7] are given in Table X. As in the presentation of the tritium-production results, the results of the activation calculations are given as the ratio of the experiment to calculation and the quoted errors are due to the experimental uncertainties only.

A. The (n,2n) Activations

The (n,2n) activations of six different targets were observed. The (n,2n) reactions considered here have threshold energies ranging from ~8 to 12 MeV, except for ^{238}U, which has a threshold of 6.17 MeV. These activations consequently result largely from the unattenuated 14-MeV component of the neutron spectra at the various radii. Comparison of the calculations with the measurements provides a test of how well the transport codes treat 14-MeV neutron attenuation.

In Table XI, we give the ^{89}Y(n,2n) activation results for the four calculations, which are typical of all the (n,2n) results. Table XII gives the results of Calculation IV for all activations. These results are shown in Figs. 4-10. From Table XI, we see that there is generally good agreement between the experiment and the two Monte Carlo calculations. The S_n calculations give less satisfactory agreement with the experiment. This is due in part to streaming effects in the S_n method, which does not permit precisely radial transport. The large discrepancies at the smallest radial source distance (22.2 mm), which occur in all the calculations, are thought to come from a slightly off-center source. The neutron

TABLE X

RADIOCHEMICAL-ACTIVATION DATA[a] (10^{13})

Reaction	Distance From Source					
	22.2 mm	50.0 mm	76.15 mm	126.0 mm	200.0 mm	300.0 mm
$^{89}Y(n,2n)^{88}Y$	1665	219.2	76.25	18.02	3.999	0.6924
$^{90}Zr(n,2n)^{89}Zr$		145.0	49.78	11.44	2.131 ± 4%	0.3561 ± 9%
$^{169}Tm(n,2n)^{168}Tm$		528.6	197.4	55.00	13.62	2.935
$^{191}Ir(n,2n)^{190}Ir$		534.7	197.6	51.15	12.70	2.660 ± 7%
$^{197}Au(n,2n)^{196}Au$	3916	578.3	214.8	56.88	13.87	2.994
$^{238}U(n,2n)^{237}U$	1540	295.9	118.7	37.13	10.88	2.733 ± 5%
$^{193}Ir(n,2n)^{192}Ir$ + $^{191}Ir(n,\gamma)^{192}Ir$		401.1	166.8	52.30	16.20	2.97 ± 7%
$^{193}Ir(n,n')^{193m}Ir$		61 ± 15%	33 ± 25%	15 ± 50%	8 ± 100%	
$^{235}U(n,f)^{99}Mo$		829	374	142	46.0	8.62 ± 4%
$^{238}U(n,f)^{99}Mo$	2285	369	150	46.7	13.0 ± 4%	3.26 ± 5%
$^{45}Sc(n,\gamma)^{46}Sc$		3.508	2.492	1.363	0.5511	0.0971 ± 7%
$^{89}Y(n,\gamma)^{90}Y$	4.592	2.029	1.310	0.6687	0.2562	0.03483
$^{169}Tm(n,\gamma)^{170}Tm$		59.80	44.75	24.38	10.04	1.974 ± 10%
$^{197}Au(n,\gamma)^{198}Au$	72.35	50.63	36.44	19.81	8.126	1.068
$^{238}U(n,\gamma)^{239}U$	46.11	29.75	20.87	11.14	4.476	0.5841

[a]Unless otherwise specified, the precision of the data is ±3%.

TABLE XI

RATIO OF OBSERVED-TO-CALCULATED $^{89}Y(n,2n)^{88}Y$ ACTIVATIONS

Calculation	Distance From Source					
	22.2 mm	50.0 mm	76.15 mm	126.0 mm	200.0 mm	300.0 mm
I	0.752	0.740	0.726	0.740	0.803	0.934
II	0.936	0.926	0.883	0.847	0.848	0.924
III	1.008	1.067	0.993	0.964	0.938	1.048
IV	1.026	1.059	1.041	0.983	0.964	1.079

spectrum at this point consists mainly of the unattenuated 14-MeV component. There is also a low-energy component from backscattered neutrons, but this contributed negligibly to the (n,2n) activations. Moreover, the (n,2n) activation cross sections are generally known to within a few per cent in the required energy range. Hence, we disregard the discrepancies at 22.2 mm. At the other radii, Calculation IV seems to be in generally good agreement with the experiment. Most of the remaining discrepancies can plausibly be attributed to errors in the activation cross sections. However, the results do suggest that there may be some small errors in the total cross sections for ^{6}Li or deuterium in the 14-MeV region. This is surmised because the observed-to-calculated ratio for a given activation generally decreases with

TABLE XII

RATIO OF OBSERVED-TO-CALCULATED RADIOCHEMICAL ACTIVATIONS (CALCULATION IV)

Reaction	Distance From Source					
	22.2 mm	50.0 mm	76.15 mm	126.0 mm	200.0 mm	300.0 mm
$^{89}Y(n,2n)^{88}Y$	1.256	1.035	1.039	0.984	1.020	0.966
$^{90}Zr(n,2n)^{89}Zr$		0.983	0.992	0.941	0.849	0.819
$^{169}Tm(n,2n)^{168}Tm$		1.004	0.997	1.003	0.992	0.973
$^{191}Ir(n,2n)^{190}Ir$		0.999	0.984	0.921	0.916	0.875
$^{197}Au(n,2n)^{196}Au$	1.135	0.979	0.974	0.939	0.925	0.919
$^{238}U(n,2n)^{237}U$	1.136	1.102	1.057	1.032	1.058	1.085
$^{193}Ir(n,2n)^{192}Ir$ + $^{191}Ir(n,\gamma)^{192}Ir$		1.061	1.062	0.994	1.007	1.046
$^{193}Ir(n,n')^{193m}Ir$		0.744	0.793	0.908	1.453	
$^{235}U(n,f)^{99}Mo$		1.030	1.001	1.004	0.989	1.047
$^{238}U(n,f)^{99}Mo$	1.163	0.992	0.999	0.998	0.995	1.121
$^{45}Sc(n,\gamma)^{46}Sc$		1.054	1.077	1.084	1.085	1.438
$^{89}Y(n,\gamma)^{90}Y$	0.971	1.015	1.028	1.011	0.978	0.991
$^{169}Tm(n,\gamma)^{170}Tm$		0.962	0.943	0.878	0.860	1.404
$^{197}Au(n,\gamma)^{198}Au$	1.026	1.059	1.041	0.983	0.964	1.079
$^{238}U(n,\gamma)^{239}U$	1.438	1.243	1.189	1.129	1.107	1.166

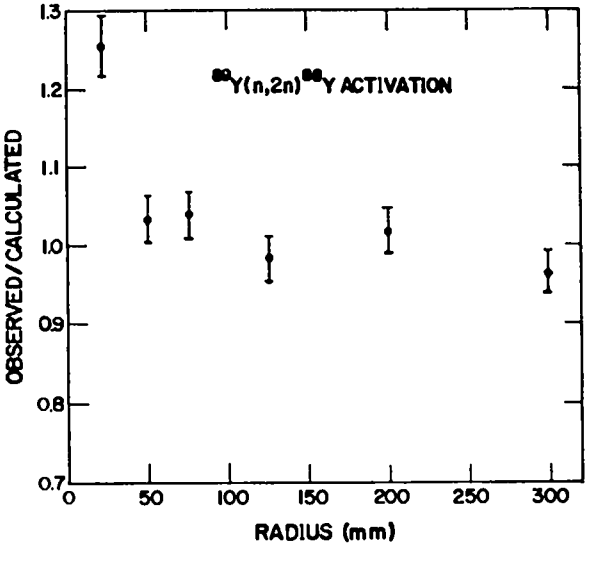

Fig. 4.
Ratio of observed-to-calculated $^{89}Y(n,2n)^{88}Y$ activation vs radius. The error bars are from experimental uncertainties only. The threshold energy is 11.60 MeV.

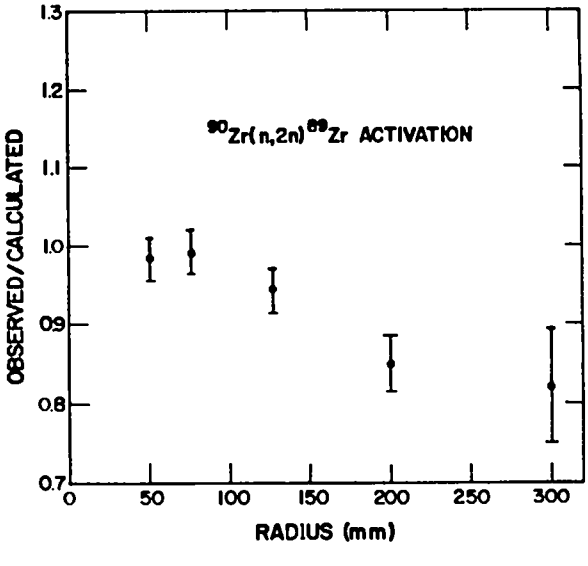

Fig. 5.
Ratio of observed-to-calculated $^{90}Zr(n,2n)^{89}Zr$ activation vs radius. The error bars are from experimental uncertainties only. The threshold energy is 12.12 MeV.

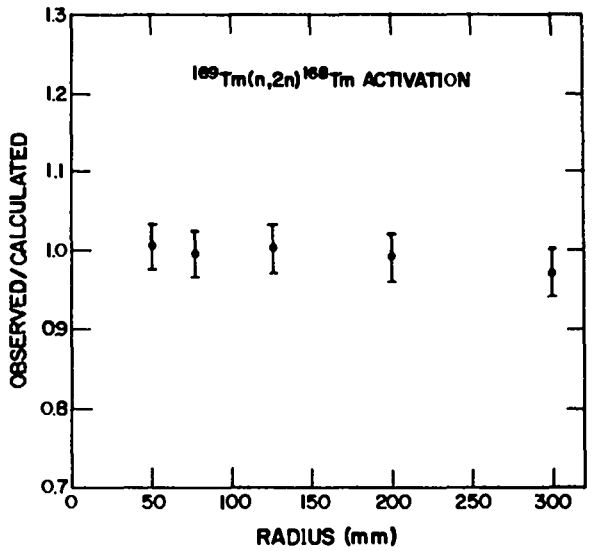

Fig. 6.
Ratio of observed-to-calculated $^{169}Tm(n,2n)^{168}Tm$ activation vs radius. The error bars are from experimental uncertainties only. The threshold energy is 8.11 MeV.

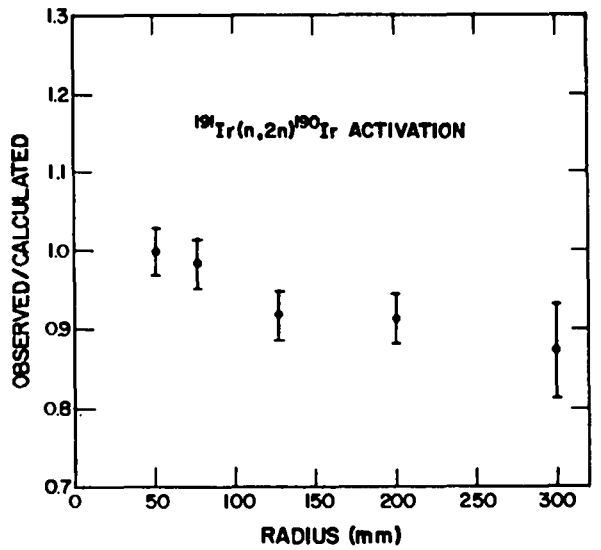

Fig. 7.
Ratio of observed-to-calculated $^{191}Ir(n,2n)^{190}Ir$ activation vs radius. The error bars are from experimental uncertainties only. The threshold energy is 8.17 MeV.

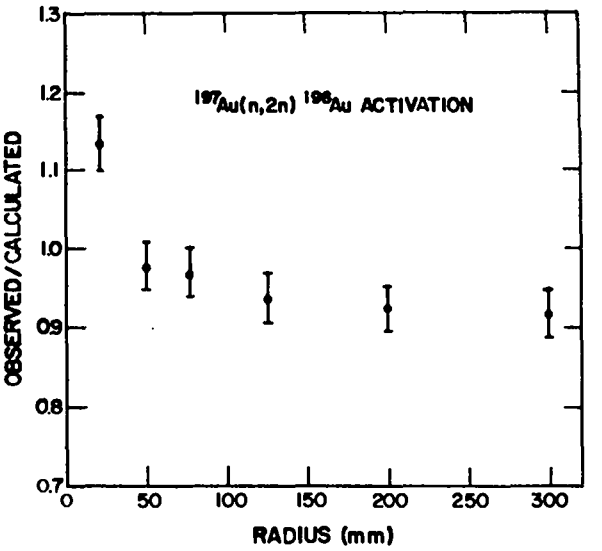

Fig. 8.
Ratio of observed-to-calculated $^{197}Au(n,2n)^{196}Au$ activation vs radius. The error bars are from experimental uncertainties only. The threshold energy is 8.12 MeV.

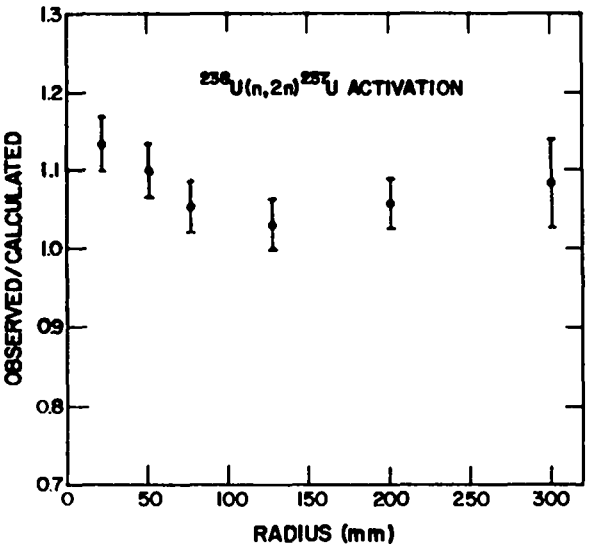

Fig. 9.
Ratio of observed-to-calculated $^{238}U(n,2n)^{237}U$ activation vs radius. The error bars are from experimental uncertainties only. The threshold energy is 6.17 MeV.

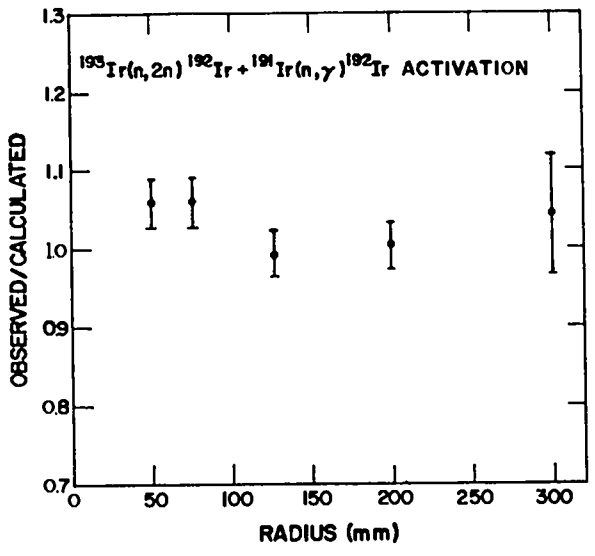

Fig. 10.
Ratio of observed-to-calculated $^{193}Ir(n,2n)^{192}Ir + ^{191}Ir(n,\gamma)^{192}Ir$ activation vs radius. The error bars are from experimental uncertainties only.

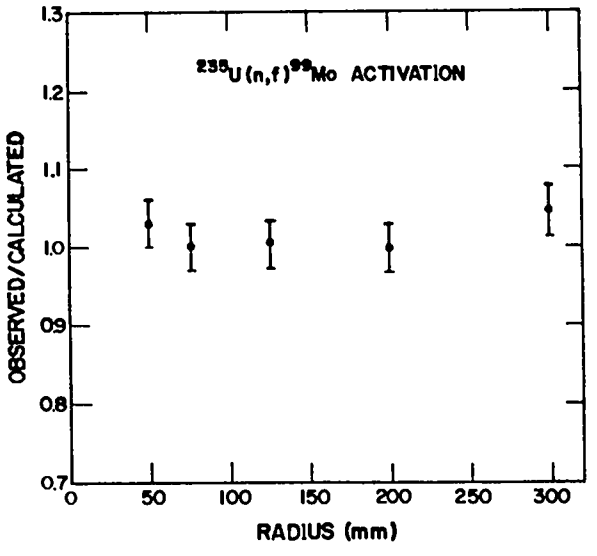

Fig. 11.
Ratio of observed-to-calculated $^{235}U(n,f)^{99}Mo$ activation vs radius. The error bars are from experimental uncertainties only.

increasing radial source distance. This behavior is particularly pronounced for the highest threshold target, ^{90}Zr (threshold energy 12.12 MeV), and is essentially absent from the $^{238}U(n,2n)$ results, which have a significantly larger contribution from down-scattered neutrons at the larger radii. Optimum agreement between the (n,2n) data and calculations is obtained by an upward rescaling of all ^{6}Li or deuterium cross sections by 4 and 3%, respectively, in the 14-MeV region. The production of ^{192}Ir is due to both (n,2n) and (n,γ) reactions. The $^{193}Ir(n,2n)^{192}Ir$ reaction contributes more than 70% to the total, except at 200 mm where the contribution is ~55%.

B. The (n,f) Activations

The (n,f) activations of ^{235}U and ^{238}U were observed. The $^{238}U(n,f)$ reaction has an effective threshold of ~1 MeV with most of the activation resulting from neutrons above 5 MeV. The reaction cross section is thus similar to that of the $^{238}U(n,2n)$ and $^{7}Li(n,n'\alpha)$ reactions. The results of Calculation IV are given in Table XII and shown in Figs. 11 and 12. Disregarding the 22.2-mm data, Calculation IV

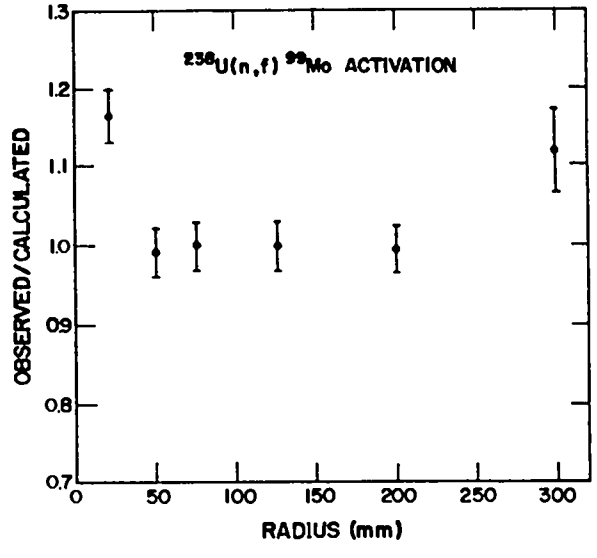

Fig. 12.
Ratio of observed-to-calculated $^{238}U(n,f)^{99}Mo$ activation vs radius. The error bars are from experimental uncertainties only.

is in satisfactory agreement with experiment, except possibly at the 300-mm radius at the outside of the LiD sphere. The reason for this discrepancy is not clear, because the fission cross section is thought to be known to within a few per cent.

The $^{235}U(n,f)$ activation is due to the entire neutron energy spectrum present in this experiment. It is the first radiochemical activation discussed so far that probes the lower energy region of the spectrum. Calculation IV and the experiment are in satisfactory agreement everywhere.

The two Monte Carlo calculations give (n,f) activations that agree everywhere within 1%. The two S_n calculations are not in such close agreement with each other or with the Monte Carlo results. Calculation II, the most reliable S_n computation, is in somewhat better agreement with the experiment than Calculation I is. The $^{235}U(n,f)$ results for the various calculations are given in Table XIII. The $^{238}U(n,f)$ results are similar.

C. The (n,γ) Activations

The (n,γ) activations of five different target nuclei were measured in this experiment. The (n,γ) cross sections for these targets generally rise rapidly with decreasing energy, so that these activations come primarily from the lower energy range of the neutron spectra. Typically 70% of the activations come from neutron energies less than 70 keV, except at the 22.2-mm radius where there is a significant 14-MeV contribution. These activations provide a stringent test of the transport codes, because the lower energy region of the neutron spectrum is populated through successive downscattering interactions. Unfortunately, the (n,γ) reaction cross sections for most of the target nuclei used are not well known.

The results of Calculation IV are given in Table XII and shown in Figs. 13-17. Only for gold, whose activation cross section is thought to be well known, are Calculation IV and the experiment in satisfactory agreement everywhere. Satisfactory agreement for scandium, yttrium, and thulium is also obtained everywhere except possibly at the 300-mm position,

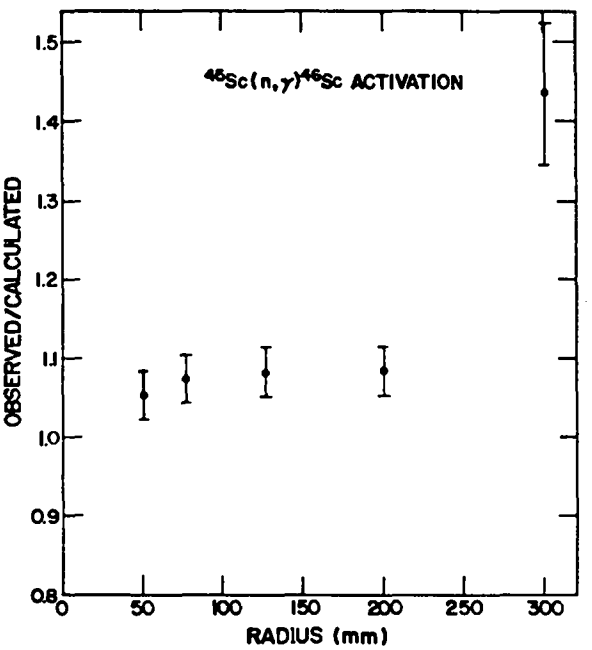

Fig. 13.
Ratio of observed-to-calculated $^{45}Sc(n,\gamma)^{46}Sc$ activation vs radius. The error bars are from experimental uncertainties only.

TABLE XIII

RATIO OF OBSERVED-TO-CALCULATED $^{235}U(n,f)^{99}Mo$ ACTIVATIONS

	Distance From Source				
Calculation	**50.0 mm**	**76.15 mm**	**126.0 mm**	**200.0 mm**	**300.0 mm**
I	0.880	0.844	0.879	0.925	1.099
II	0.964	0.908	0.904	0.888	0.968
III	1.036	0.990	1.000	0.978	1.039
IV	1.030	1.001	1.004	0.989	1.047

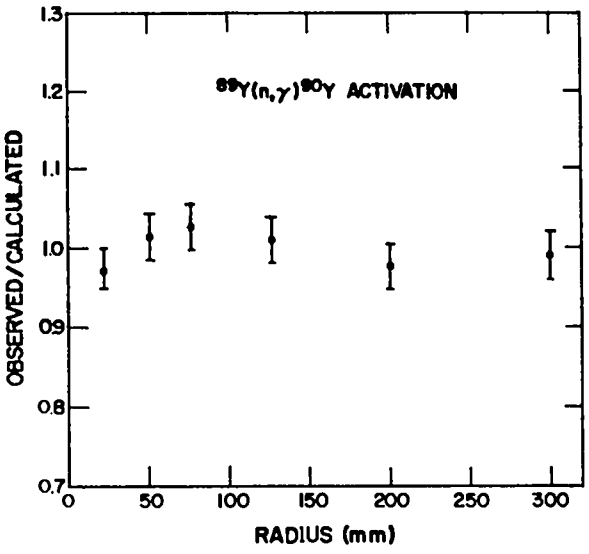

Fig. 14.
Ratio of observed-to-calculated $^{89}Y(n,\gamma)^{90}Y$ activation vs radius. The error bars are from experimental uncertainties only.

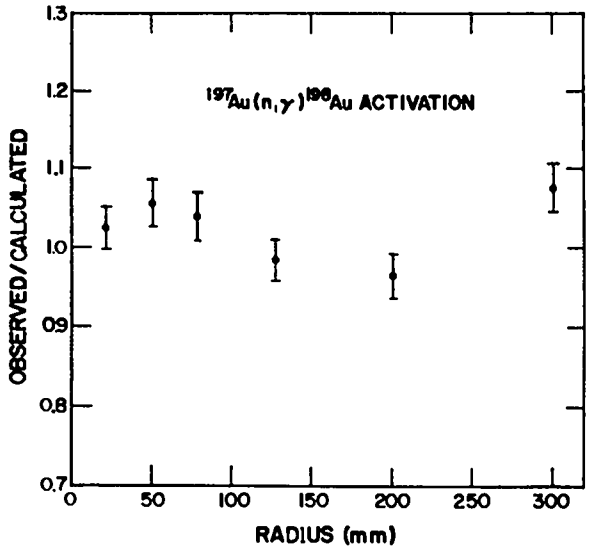

Fig. 16.
Ratio of observed-to-calculated $^{197}Au(n,\gamma)^{198}Au$ activation vs radius. The error bars are from experimental uncertainties only.

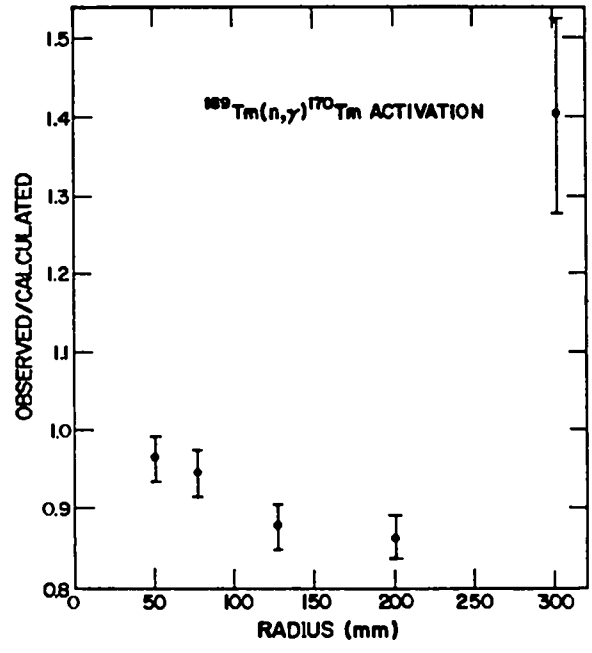

Fig. 15.
Ratio of observed-to-calculated $^{169}Tm(n,\gamma)^{170}Tm$ activation vs radius. The error bars are from experimental uncertainties only.

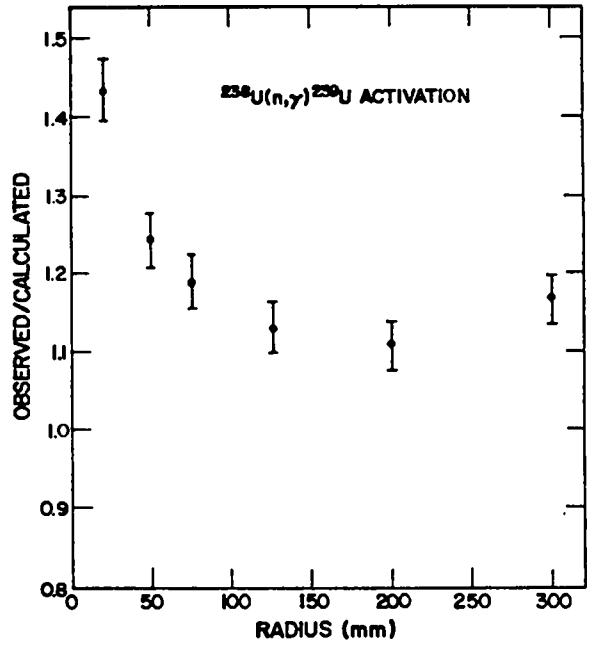

Fig. 17.
Ratio of observed-to-calculated $^{238}U(n,\gamma)^{239}U$ activation vs radius. The error bars are from experimental uncertainties only.

where there are rather large discrepancies in the scandium and thulium results. The calculated $^{238}U(n,\gamma)$ activations are everywhere smaller than observed (generally by 10 to 20%), suggesting that the activation cross section used is too small, particularly in the 14-MeV region, because the discrepancy is even larger at 22.2 mm. Note that the postulated off-center position of the experimental source is not expected to influence the (n,γ) activations at 22.2 mm by more than a few per cent. Finally, the fact that the observed-to-calculated activation ratio is generally large at 300 mm, the outside position, suggests that there may be some room return, which has been neglected in the calculations. A calculation that attempted to simulate the room return, however, failed to significantly modify the results. Moreover, if sufficient room return were present to explain the scandium and thulium discrepancies, a large discrepancy would then be introduced in the gold results at 300 mm because of the large value of the $Au(n,\gamma)$ cross section at very low energies.

As for the (n,f) activations, the two Monte Carlo calculations are in very close agreement. This is not surprising because Calculation III is used to provide the lower energy fluences for Calculation IV. The two S_n calculations are in much poorer agreement with the experiment; the more reliable 21-group calculation gives somewhat better results. The results of the four calculations of the $Au(n,\gamma)$ activations, which are typical, are given in Table XIV.

D. The $^{193}Ir(n,n')^{193m}Ir$ Activation

The cross section for the $^{193}Ir(n,n')^{193m}Ir$ reaction is very poorly known. Consequently, we consider Calculation IV to be in satisfactory agreement with the experiment (see Table XII).

V. CONCLUSIONS

It seems, on the basis of this experiment, that our understanding of neutron transport through ^6LiD is essentially correct. In most cases, discrepancies between calculation and experiment can be plausibly explained in terms of imprecisely known cross sections. The cross-section data relevant to transport through ^6LiD appear to be essentially correct, although there is some indication that the 14-MeV inelastic or nonforward elastic cross sections on deuterium and/or ^6Li may be a few per cent too small. The cross-section data used for the (n,2n) and (n,f) activations seem to be basically correct. Except for $^{238}U(n,\gamma)$, the (n,γ) activation cross sections also seem to be reasonably accurate, even though only the cross sections for gold are well known experimentally. The $^7Li(n,n'\alpha)$ cross-section data are quite possibly in error (too high) by ~15% in the 14-MeV region, whereas the $^6Li(n,\alpha)$ cross sections seem to be quite accurate.

For neutron-transport computations, the Monte Carlo methods provide more realistic results than do

TABLE XIV

RATIO OF OBSERVED-TO-CALCULATED $^{197}Au(n,\gamma)^{198}Au$ ACTIVATIONS

	Distance From Source					
Calculation	22.2 mm	50.0 mm	76.15 mm	126.0 mm	200.0 mm	300.0 mm
I	0.752	0.740	0.726	0.740	0.803	0.934
II	0.936	0.926	0.883	0.847	0.848	0.924
III	1.008	1.067	0.993	0.964	0.938	1.048
IV	1.026	1.059	1.041	0.983	0.964	1.079

the S_n techniques, although they require significantly more machine time. It is reassuring that our most realistic simulation of the experiment, Calculation IV, provides the best overall fit to the data. We believe that further improvement in the calculation could be obtained only with the incorporation of improved nuclear data.

ACKNOWLEDGMENTS

I would like to thank the following people for useful discussions and encouragement: D. W. Barr, D. W. Muir, W. E. Preeg, J. C. Solem, and P. P. Whalen. Particular thanks are due to J. S. Hendricks, who compiled the radiochemical-activation cross-section data and evaluated the radiochemical-activation integrals. Those who participated in the radiochemical-activation experiment were D. W. Barr, G. W. Knobelock, B. P. Bayhurst, R. J. Prestwood, J. S. Gilmore, K. Wolfsberg, G. P. Ford, V. M. Armijo, T. D. Baker, J. E. Hasty, and J. Drake.

REFERENCES

1. J. S. Hendricks, Los Alamos Scientific Laboratory internal document (May 14, 1976).

2. L. L. Carter, E. D. Cashwell, C. J. Everett, C. A. Forest, R. G. Schrandt, W. M. Taylor, W. L. Thompson, and G. D. Turner, "Monte Carlo Code Development in Los Alamos," Los Alamos Scientific Laboratory report LA-5903-MS (March 1975).

3. E. D. Cashwell, J. R. Neergaard, W. M. Taylor, and G. D. Turner, "MCN: A Neutron Monte Carlo Code," Los Alamos Scientific Laboratory report LA-4751 (January 1972).

4. D. W. Muir and M. E. Wyman, "A Tritium-Production Measurement with Application to Fusion Reactor Blanket Design," Trans. Am. Nucl. Soc. 15, 631 (1972).

5. W. A. Reupke and D. W. Muir, "Neutronic Data Consistency Analysis for Lithium Blanket and Shield Design," 2nd Top. Meet. Technol. Control. Nucl. Fusion, Richland, Washington, September 21-23, 1976 (Electric Power Research Institute, Palo Alto, CA 94304).

6. W. A. Reupke, "The Consistency of Differential and Integral Thermonuclear Neutronics Data," (Ph.D. thesis, Georgia Institute of Technology, Atlanta, GA 30332, 1977), Los Alamos Scientific Laboratory report LA-7067-T (January 1978).

7. D. W. Barr, Los Alamos Scientific Laboratory internal document (May 27, 1976).

Printed in the United States of America. Available from
National Technical Information Service
US Department of Commerce
5285 Port Royal Road
Springfield, VA 22161

Microfiche $3.00

001-025	4.00	126-150	7.25	251-275	10.75	376-400	13.00	501-525	15.25
026-050	4.50	151-175	8.00	276-300	11.00	401-425	13.25	526-550	15.50
051-075	5.25	176-200	9.00	301-325	11.75	426-450	14.00	551-575	16.25
076-100	6.00	201-225	9.25	326-350	12.00	451-475	14.50	576-600	16.50
101-125	6.50	226-250	9.50	351-375	12.50	476-500	15.00	601-up	

Note: Add $2.50 for each additional 100-page increment from 601 pages up.